Available online at www.sciencedirect.com

ScienceDirect

Geochimica et Cosmochimica Acta 325 (2022) 232–257

Geochimica et Cosmochimica Acta

www.elsevier.com/locate/gca

Tektite glasses from Belize, Central America: Petrography, geochemistry, and search for a possible meteoritic component

Christian Koeberl [a,*], Billy P. Glass [b], Toni Schulz [a,c], Wencke Wegner [a,d], Gabriele Giuli [e], Maria Rita Cicconi [e,1], Angela Trapananti [e], Paola Stabile [e], Mariangela Cestelli-Guidi [f], Jisun Park [g,h,i], Gregory F. Herzog [h], Marc W. Caffee [j]

[a] *Department of Lithospheric Research, University of Vienna, Althanstrasse 14, 1090 Vienna, Austria*
[b] *Department of Earth Sciences, University of Delaware, Newark, DE 19716, USA*
[c] *Institute for Geology und Mineralogy, University of Cologne, Zülpicher Strasse 49b, 50674 Cologne, Germany*
[d] *Natural History Museum, Burgring 7, 1010 Vienna, Austria*
[e] *Universita' di Camerino, Scuola di Scienze e Tecnologie, Via Gentile III da Varano, 62032 Camerino, MC, Italy*
[f] *Istituto Nazionale di Fisica Nucleare, Laboratori Nazionali di Frascati, Via Enrico Fermi 54, 00044 Frascati, Italy*
[g] *Department of Physical Sciences, Kingsborough Community College, Brooklyn, NY 11235, USA*
[h] *Department of Chemistry and Chemical Biology, Rutgers University, Piscataway, NJ 08854, USA*
[i] *Department of Earth & Planetary Sciences, American Museum of Natural History, New York, NY 10024, USA*
[j] *Department of Physics and Astronomy, and Department of Earth, Atmospheric, and Planetary Sciences, Purdue University, West Lafayette, IN 47907-2036, USA*

Received 27 September 2021; accepted in revised form 17 February 2022; Available online 22 February 2022

Abstract

The presence of tektite-like glasses from a geographically restricted area in Belize (Central America) has been known for several decades. We comprehensively studied 18 such Belize glasses by a variety of petrographic and geochemical methods, including major and trace element analysis, radiogenic isotopic composition (Rb-Sr, Sm-Nd, and Re-Os), water content, oxidation state, and cosmogenic radionuclides. The aims were to determine their compositional variation, their mode of formation and possible source rocks, and their relation to known tektites, and to search for evidence of an extraterrestrial component.

In terms of petrography, the samples are similar to tektites from the four "classical" strewn fields, with the presence of lechatelierites, schlieren, and vesicles; these are also widely accepted indicators of an impact origin. No close similarities to volcanic glasses are evident. Water contents are very low, and iron oxidation states are mostly reduced, in both cases similar to observations for other tektites. The geochemical and isotopic data presented, such as Cr, Co and Ni elemental abundances and interelement ratios, as well as trace element patterns are typical for local and regional volcanics from the active Central American Arc. Particular similarities to material comparable to volcanic rocks from Honduras or Guatemala are noted. This is confirmed by Sr-Nd isotope signatures of the Belize glasses, showing close similarities to Central American volcanics in general, and Honduran and Guatemalan volcanic, in particular. Osmium concentrations and $^{187}Os/^{188}Os$ ratios are comparable to arc volcanics from world-wide locations, but - in a few of the samples - elevated Ir concentrations, near-chondritic Pt/Ir and $^{187}Os/^{188}Os$ ratios can also be interpreted with the admixture of a minor meteoritic component to some of the Belize

* Corresponding author.
E-mail address: christian.koeberl@univie.ac.at (C. Koeberl).
[1] Current address: Department Werkstoffwissenschaften, Lehrstuhl für Glas und Keramik, Universität Erlangen-Nürnberg, Martensstrasse 5, D-91058 Erlangen, Germany.

https://doi.org/10.1016/j.gca.2022.02.021
0016-7037/

samples. ^{10}Be concentrations are consistent with values typical of both, young or deeply buried soils and with values for Central American volcanics, which carry subducted ^{10}Be.

Geochemical data clearly indicate a source different from that of the Australasian tektites. Both isotope data sets for the Belize glasses indicate a close relationship to local arc lavas, especially those from Guatemala and Honduras, suggesting that the glasses were not deposited very far from their source. The main evidence that the Belize glasses are of impact origin are their petrographic characteristics and low water content. The evidence from ^{10}Be is consistent with, but does not require, a model of formation for the Belize glasses by an impact on loosely consolidated surface sediments exposed to rain. A probable meteoritic component is low and heterogeneously distributed.

Keywords: Impact glass; Belize; Tektites

1. INTRODUCTION

Tektites are natural glasses on Earth of up to a few cm in size that occur mostly in four geographically extended (but well-defined) strewn fields: the North American strewn field of 35.5 Ma age (associated with the Chesapeake Bay impact structure; cf. Poag et al., 2004); the Central European strewn field of ca. 14.8 Ma age (associated with the Ries crater in southern Germany); the Ivory Coast tektite strewn field of 1.1 Ma (derived from the Bosumtwi impact structure in Ghana); and the 0.79 Ma Australasian strewn field (for which no undisputed source crater has been identified so far); see Fig. 1a. For details on these strewn fields and the chemistry and origin of the tektites, see the reviews in, e.g., Koeberl (1994, 2014). It is well established that the chemical and the isotopic composition of tektites in general are identical to those of the terrestrial upper continental crust (see, e.g., Blum et al., 1992, and reviews in e.g., Koeberl, 1994, 2014, and references therein).

A detailed discussion of tektite characteristics is given by Koeberl (2014). For our purposes the important properties of true tektites are: (1) they are glassy (amorphous); (2) they are fairly homogeneous rock (not mineral) melts; (3) they contain abundant lechatelierite; (4) they occur in geographically extended strewn fields (not just at one or two closely related locations); (5) they are distal ejecta and are not found in or around a source crater, or within typical impact lithologies (e.g., suevitic breccias, impact melt breccias); (6) they generally have low water contents and a very small extraterrestrial component; and (7) they are interpreted to have formed from the uppermost layer of the target surface, as is indicated by the ^{10}Be content of Australasian, Ivory Coast, and Central European tektites. This ^{10}Be was not produced by direct, *in-situ* irradiation with cosmic rays in space or on Earth but was inherited from sediments, where it was produced by neutron reactions on oxygen in the atmosphere; such ^{10}Be is often termed meteoric or garden variety. It is recommended that the term "tektite" should only be used for glasses that have (most) of the above characteristics listed; if not, or if the data are still ambiguous, the more general term "impact glass" for objects that mainly satisfy all criteria but numbers 4, 5, and 7 is more appropriate.

Within the past 20–30 years or so, glasses with some of these properties (as listed above) have been reported from western Belize, possibly indicating a new tektite strewn field in Central America. Approximately 7000 of these objects have been found to date in west central Belize since 1990 (references see below; the following description is based on personal information by J. Cornec to B. Glass, except as referenced). The total area of the strewn field (Fig. 1b) is about 500 km^2. Belize glasses are found in the NW part of the Cayo District, erratically distributed within the following geologic sequences: (1) Upper Quaternary-age lag gravels, (2) a series of Quaternary gravel beds, and (3) in lag gravels on top of the Red Bank group (which was earlier assumed to be of Miocene age but has recently been shown to be to be upper Paleocene to lower Eocene in age; cf. King et al., 2018; Ricketts et al., 2021). Typically, glasses are found on surface exposures of Upper Quaternary-age lag gravels where erosion has removed fine material and left coarser fragments as a lag. These surfaces are developed over the Red Bank group clays. Quaternary gravel beds occur on Upper Quaternary-age river terraces that outcrop north of the Belize River, particularly from the Buena Vista/Iguana Creek area westward to Santa Familia. The glasses recovered from these gravel beds show signs of transport and are usually quite rounded, smooth and shiny. Identical gravel beds found in La Democracia, Burrell Boom, and West of Blue Creek near the Mexican border appear to be devoid of tektites. Glasses are found embedded in the very top of montmorrilonitic (Ricketts et al., 2021) clay units of the Red Bank group, but exact age constraint is lacking.

It is difficult to establish with certainty the *in situ* location of the glasses, i.e., if they have been in the same rock layer since they were deposited. They are usually masked by a thin overlying organic soil horizon. They have been collected in road and drainage ditches, the edges of cattle ponds, in gullies and in small stream beds, and occasionally at the surface of plowed fields. They are not distributed evenly but tend to be found in patches while nearby, seemingly identical areas appear completely barren. Recent deforestation for agricultural development is now revealing these objects for the first time. Few additional finds are expected any time soon, as jungle marks part of the known boundary of much of the strewn field.

The Belize glasses are mostly in the 1–3 cm size range and they range in mass from < 1 up to $\sim$103 grams; the largest is spherical in shape. They are black in reflected light. Most ($\sim$80 %) are spherical, but rotational forms have also been found. Teardrops plus dumbbells make up

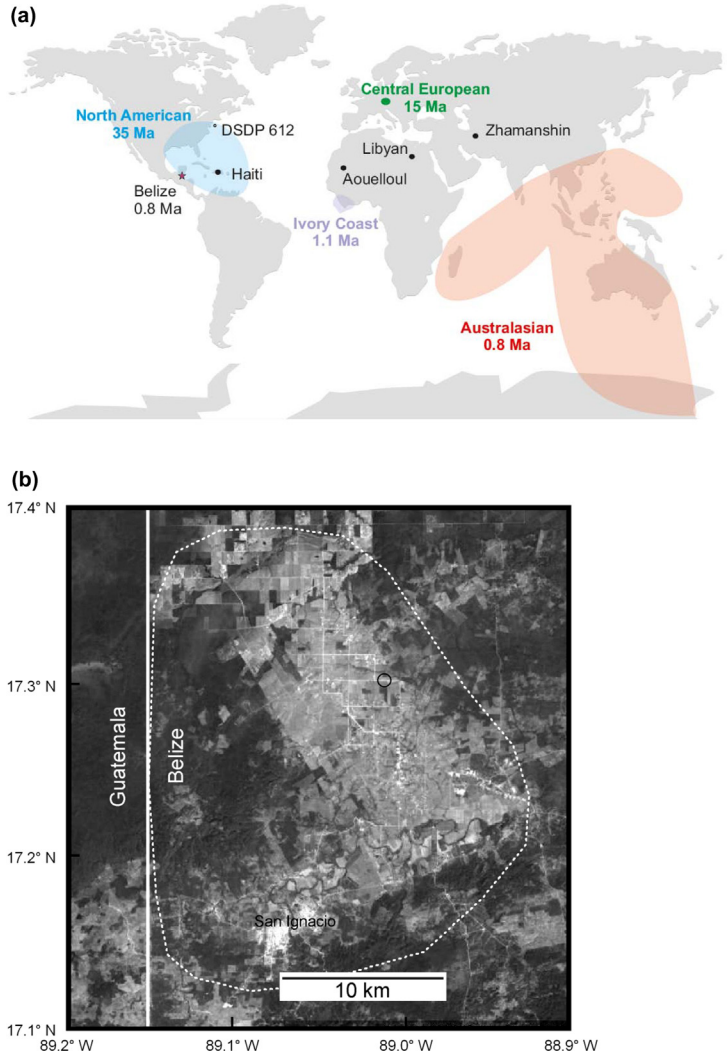

Fig. 1. (a) World map showing the four traditional extended tektite strewn fields, as well as the locations of some other impact glass occurrences, and the Belize location. (b) Map of the Belize strewn field. The region where the Belize specimens have been recovered is outlined with a white dashed line. The apparent western boundary of the strewn field is adjacent to the border between Belize and Guatemala. The town of San Ignacio is in the southern part of the strewn field. The black circle near 17.3° north latitude and 89° west longitude is the area where the specimens in this study were found.

~1 % and discs make up ~2–3 %. The remaining ~16 % of the non-spherical objects are fragments of the spherical ones or are irregular in shape. The tektites that have not been abraded excessively generally exhibit pitting, U-shape grooves, and striations.

Our earlier work on the Belize glasses has been reported in abstract form from 2014 to 2018. Other important information, on the distribution, stratigraphy, and petrographic characteristics of these materials, is available only in abstract format (Povenmire et al., 2011, 2012, 2014; Cornec et al., 2013; Povenmire and Cornec, 2015; Povenmire, 2016; and King et al., 2016a,b). The earlier discovery of a few tektite-like glasses at the archeological site of Tikal in Guatemala was later linked to the source region in Belize (Hildebrand et al., 1994; Senftle et al., 2000). Measurements of magnetic properties of Belize glasses by Rochette et al. (2015) noted similarities to Darwin glass (an impact glass). Several glasses from Belize were dated by the ^{40}Ar-^{39}Ar method, giving total fusion ages of 820 ± 40 ka (2σ) (Izett and Meeker, 1995). Schwarz et al. (2016) reported a ^{40}Ar/^{39}Ar plateau age of 769 ± 16 ka for one sample. More recently, Rochette et al. (2021) reported a variety of data on Belize glasses, including an updated age of 804 ± 9 ka, and suggested a link to the so-called Pantasma structure in Nicaragua.

The present study aims to characterize the glasses from Belize petrographically and geochemically – including isotopic analyses – to better constrain the nature of their precursor rocks, possibly local lavas from the active Central American arc. A meteoritic impact origin of the Belize glasses is supported by several lines of evidence, including their low water content, petrographic observations (e.g., the absence of primary crystallites/microlites, the presence of lechatelierite), and the extent of the strewn area

(e.g., Povenmire et al., 2011). In addition to geochemical and Sr-Nd isotope data, we present concentrations for selected highly siderophile elements (HSEs; Re, Os, Ir and Pt) and $^{187}Os/^{188}Os$ isotopic signatures, which represent a useful tool in the detection of even minor (sub-percent level) extraterrestrial admixtures. We compare our results to other impact glasses (Australasian-, Ivory Coast-, and Central European tektites, and irghizites) for which a meteoritic component was postulated based on HSE and $^{187}Os/^{188}Os$ data (e.g., Koeberl and Shirey, 1993; Jonášová et al., 2016; Ackerman et al., 2017, 2019). We also investigated the iron oxidation state, the water content, and the ^{10}Be content of selected samples, to further constrain their origin and possible source material.

2. SAMPLES AND METHODS

2.1. Samples

We studied 18 Belize glasses collected within an area of about a square kilometer centered at ~17.30° north latitude and ~89.01° west longitude (Fig. 1b); the samples were provided to us by J. Cornec, who owns most of the about 7000 such samples found so far (see references in previous section). They ranged in mass from 1.306 g to 9.020 g (Table 1). The larger ones were usually rounded in shape and the smaller ones had irregular shapes and were probably fragments. One had a flat teardrop shape, two others were roughly teardrop shaped, and two were oval in shape. Most of the specimens exhibited some abrasion, indicating that they had been transported, possibly by rivers or streams. All of the samples had pits on at least part of their surface. The larger pits on five of the specimens had smaller pits superimposed on them. Overlapping, fine (<1 μm size) pits on the surface of one tektite (B13) produced a dull or matted surface. About half of the larger (>3 grams) tektites had U-shaped grooves on their surfaces, while only one of the smaller (<3 grams) tektites had U-shaped grooves (Table 1). Eight out of the 18 tektites had striations etched into their surfaces. One specimen (the second largest) had percussion marks on its surface. About one third were deeply etched in places. Three specimens had a deep groove or grooves on their surfaces. If these deep grooves are the result of widening of surface cracks due to solution, then half of the width of the grooves would indicate that amount of solution (this assumes that the solution rate would be the same on the surface as on both sides of the crack; as both sides are undergoing solution, the crack would widen twice as fast as the solution rate; see Glass, 1984). The amount of solution indicated by these deep grooves ranges from ~13 to 100 μm based on four measurements.

Table 1
Description of Belize tektites used in this study.

Specimen number	Weight (g)	Shape	Abraded	U-shaped grooves	Surface striations	Comments
B1	9.020	Rounded	Yes	Yes	No	
B2	6.963	Rounded	Yes	Rare	No	
B3	7.716	Rounded	Yes	Yes	Yes	Appears to have percussion marks
B4	5.985	Elongate	Some areas	No	Yes	Deeply etched in places
B5	5.896	Rounded	Some areas	No	No	Roughly egg-shaped
B6	4.730	Flat teardrop	No	No	Yes	
B7	3.866	Flat oval	Yes	Yes	Yes	
B8	3.973	Irregular shape	Trace	No	No	Deeply etched in places
B9	3.354	Rounded	Yes	Yes	Yes	Flatter on one side
B10	2.858	Rounded	Trace	No	No	
B11	1.831	Irregular shape	No	Yes	No	
B12	2.076	Oval	Yes	No	No	One end broken off diagonally and re-etched
B13	1.628	Irregular shape	Yes	No	No	Roughly teardrop shape; deeply etched with matted appearance
B14	1.803	Rounded	Yes	No	No	Rough teardrop shape
B15	1.364	Irregular shape	Some areas	No	Yes	
B16	1.306	Irregular shape	Some areas	No	Yes	One surface is concave; deeply etched in some areas
B17	1.365	Irregular shape	No	No	No	Elongate with the smaller end broken off; deeply etched in places
B18	1.313	Irregular shape	No	No	Yes	Deeply etched in places

Note: All tektites exhibited surface pitting and most had exposed vesicles, except B3 and B14, and perhaps B5, B7, and B9.

2.2. Methods: Petrography

Thick sections (~300 μm) were cut from each of the eighteen Belize tektites and mounted on petrographic slides for microscope work. The thick sections gave enough volume that we were able to find several rare grains that we might have missed otherwise, but were thin enough for petrographic microscope study of the sections in transmitted light. Abundances of lechatelierite and vesicles in each section were estimated by 1000 point counts on each section.

2.3. Methods: Major and trace elements

Carbon-coated polished thin sections were made from each sample and viewed with an electron microscope in secondary and in backscattered electrons. The homogeneity and composition of the impact glasses was assessed using a JXA-8530F field emission electron microprobe at the Natural History Museum in Vienna. The major element compositions were obtained using a 20 nA defocused electron beam (10 μm) accelerated to 15 kV. Major element contents were measured by wavelength-dispersive spectrometry based on back-scattered electron images (BSE) from point measurements on polished thin sections. Measurement points were selected to include the gray scale levels of the BSE images (analogues for atomic number) that correspond to the range of phases observed in the specific glasses.

Trace element concentrations in all Belize tektite samples (B1-B18) were determined by Instrumental Neutron Activation Analysis (INAA) at the Department of Lithospheric Research, University of Vienna. Samples weighing about 100 mg, along with ~90 mg of three international rock standards (the carbonaceous chondrite Allende, Smithsonian Institution, Washington DC, USA, Jarosewich et al. 1987; the Ailsa Craig Granite AC-E, Centre de Recherche Petrographique et Geochimique, Nancy, France, Govindaraju, 1989; and the Devonian Ohio Shale SDO-1, United States Geological Survey, Govindaraju, 1989) were sealed in polyethylene capsules and irradiated in the 250 kW Triga Mark-II reactor at the Atomic Institute of the Austrian Universities. More details on the instrumentation used, methodology precision, and accuracy are given by Koeberl (1993) and Mader and Koeberl (2009). In all cases when trace element concentrations were derived from both EMP and INAA, the two values were identical within error.

2.4. Methods: Isotope geochemistry

Isotope ratios of $^{87}Sr/^{86}Sr$ and $^{143}Nd/^{144}Nd$ were measured using a Finnigan TRITON thermal ionization mass spectrometer (TIMS) at the Laboratory of Geochronology, Department of Lithospheric Research, University of Vienna. An aliquot of each tektite was hand-ground in an agate bowl to a grain size < 63 μm. Tektites B1 to B12 were selected and ca. 50–70 mg of the sample powder was digested in Savillex beakers using 5 ml of HF: HNO_3 (4:1) for 2 weeks at 110 °C on a hot plate. After acid evaporation the residue was dissolved in 1 mL 6 M HNO_3 and after evaporation in 5 mL 6 M HCl leading to clear solutions. Strontium and REE extraction was performed using BIORAD AG 50 W-X8 (200–400 mesh) resin and 2.5 N and 4.0 N HCl as eluants. Neodymium was separated from the REE group using teflon-impregnated ion-exchanging HDEHP bis-(2-etylhexy)-phosphate and 0.24 M HCl as eluant. Maximum total procedural blanks were <1 ng for Sr and 50 pg for Nd, and thus considered negligible. The separated element fractions were loaded on Re double filaments (ca. 1 μg) and run in static mode. A mean $^{87}Sr/^{86}Sr$ ratio of 0.710254 ± 0.000003 ($n = 4$) was determined for the NBS987 (Sr) and a mean $^{143}Nd/^{144}Nd$ ratio of 0.511845 ± 0.000004 ($n = 4$) for the La Jolla (Nd) NIST standard reference materials during the period of investigation. Within-run mass fractionation was corrected for $^{88}Sr/^{86}Sr = 8.3752$, and $^{146}Nd/^{144}Nd = 0.7219$, respectively. Errors quoted represent 2σ errors of the mean.

A mass of ~0.1 to ~0.6 g of homogenized sample powder was spiked with a mixed tracer composed of ^{185}Re, ^{190}Os, ^{191}Ir, and ^{194}Pt and digested in 7 mL inverse aqua regia (HNO_3-HCl: 5 + 2 mL) acid mixture at 250 °C and 100–130 bars in an Anton-Paar high pressure asher for 12 hours. After digestion, Os was separated from the other HSEs using a $CHCl_3$/HBr liquid extraction procedure (Cohen and Waters, 1996). Osmium was further purified using a H_2SO_4/H_2CrO_4 microdistillation technique (Birck et al., 1997). After Os extraction, all other HSEs were separated using a procedure adapted from the Method of Pearson and Woodland (2000). Osmium was loaded as a bromide on Pt Ribbon filaments covered with a NaOH/$Ba(OH)_2$ activator (Luguet et al., 2008). The $^{187}Os/^{188}Os$ isotope ratio and Os concentration measurements were carried out in negative mode using a Finnigan TRITON thermal ionization mass spectrometer (TIMS) at the Department of Lithospheric Research, University of Vienna (Austria). Isobaric interferences of ^{187}Re on ^{187}Os were monitored and corrected by measuring $^{185}ReO^{3-}$ (mass 233). Mass fractionation was corrected offline using $^{192}Os/^{188}Os = 3.083$ (Völkening et al., 1991; Luguet et al., 2008). The Os total procedural blank was 0.2 pg, contributing up to 20% to some of the measured Os concentrations of the Belize glass samples.

Contents of the highly siderophile elements (HSEs) were measured using a Thermo Element XR SF-ICP-MS in single collector mode at the Steinmann-Institute at the University of Bonn (Germany), using methods described in Luguet et al. (2015). Total blanks for this study ($n = 4$) were ~4 pg for Re, ~3 pg for Ir, and ~22 pg for Pt. All reported concentration values are blank corrected.

2.5. Methods: Iron oxidation state and water content

Doubly polished slabs of about 5 × 5 × 0.5 mm were prepared for X-ray Absorption Spectroscopy (XAS) and Fourier Transform Infrared Spectroscopy (FTIR). Iron oxidation states and coordination geometry were determined by X-ray Absorption Near Edge Spectroscopy (XANES) on 13 Belize glass samples. The X-ray Absorption Spectroscopy (XAS) data were obtained at the BM08 beamline of the ESRF storage ring (Grenoble, F) using a

fixed-exit double-crystal Si (311) monochromator with a beam size at the sample of 0.30 × 1.50 mm. Harmonic rejection was achieved by using two Pd-coated mirrors working at an incidence angle of 3.6 mrad and by detuning the second monochromator crystal.

The X-ray energy was calibrated by defining the first derivative peak of a metallic Fe reference foil to be at 7112.0 eV. XAS data were recorded in step-scan mode spanning a range of ca. 500 eV across the Fe K-edge with a typical energy step of 0.15 eV in the edge region and with broader steps at higher energy with a counting time of 7 seconds per step. An average of three spectra was taken per sample. The spectra were acquired in fluorescence mode, using a 12 element ultrapure Ge multidetector; I_0 (the beam intensity) was monitored by means of an ionization chamber filled with N_2.

The experimental setting used provides an energy resolution of ~0.2 eV at the Fe K-edge. The main limitation for energy resolution is the finite core–hole width of the absorbing element (~1.15 eV at the Fe K-edge; Krause and Oliver, 1979), resulting in a convolved energy resolution (FWHM) of ~1.4 eV.

Experimental XANES spectra were reduced by background subtraction with a linear function and then normalized for atomic absorption on the average absorption coefficient of the spectral region from 7170 to 7350 eV. The threshold energy was taken as the first maximum of the first derivative of the spectra, whereas peak positions were obtained by calculating the second derivative of the spectra. Pre-edge peak analysis was carried out following the same procedure reported in Wilke et al. (2001) and Giuli et al. (2002, 2011). The pre-edge peak was fitted by a sum of pseudo-Voigt functions, and their integrated areas along with energy centroids were compared with those of the standards analyzed here and others from the literature (e.g., Wilke et al., 2001; Farges, 2001; Giuli et al., 2008, 2012) in order to extract information on Fe oxidation state and coordination number in the glasses studied. Particular care was taken in using the smallest possible number of components in the pre-edge peak fitting procedure. In particular, the number of the components was constrained to equal the number of the minima in the second derivative spectrum of the pre-edge peak. Several different procedures have been attempted for peak fitting: simultaneous fitting of the background and the pseudo-Voigt component; preliminary background subtraction followed by fitting with pseudo-Voigt component allowing the components to have different FWHM or Lorentzian character; preliminary background subtraction followed by fitting with pseudo-Voigt component constrained to have the same FWHM and Lorentzian character. The third procedure has shown to produce the best results in terms of data scatter and of agreement with independent wet-chemical titration data on synthetic glass samples (for details, see Giuli et al. 2011). Accurate analysis of the pre-edge peak energy position and integrated intensity, allowed the determination of $Fe^{3+}/(Fe^{2+} + Fe^{3+})$ ratios on all samples with an estimated error of ±0.05.

FTIR micro-spectroscopy was performed using a standard vacuum Michelson interferometer coupled to an IR microscope inside a box purged in dry nitrogen. The source was a globar Mid-IR source and the detector was a photoconductive, nitrogen-cooled Mercury Cadmium Telluride (MCT) crystal. The samples were mounted on a ZnSe polished window and placed in the focal plane of the IR microscope on a micrometric stage, where they were scanned in transmission mode with a slit aperture size of 50 μm and a 15X objective/condenser setup. The reference spectra were taken on the same ZnSe substrate.

Each spectrum was recorded in the mid-IR frequency range, averaging N = 256 scans at 2 cm^{-1} spectral resolution. The absorption band in the 3200–3600 cm^{-1} region is related to the O-H stretching mode in water and the intensity of this peak can be directly linked to the water content in the sample (Gilchrist et al., 1969).

Water contents were calculated according to the procedure by Gilchrist et al. (1969) following a standard application of the Lambert-Beer absorption law. The extinction coefficient used (74.8 cm^{-1} mol^{-1}) is in agreement with those used by Beran and Koeberl (1997) and Koeberl and Beran (1988). The density used for the water content calculation has been calculated according to Lange and Carmichael (1987) using the compositional data reported here and glass transition temperatures calculated according to Giordano et al. (2008). The densities thus calculated range between 2.417 and 2.555 g/cm^3, in agreement with published data on tektites, 2.303–2.510 g/cm^3 (King, 1964; O'Keefe, 1976; Chapman et al., 1984).

2.6. Methods: Be-10 chemical separation

Seven of the Belize glasses (B01, B03, B08, B09, B10, B11, and B12) were analyzed for ^{10}Be (half-life 1.387 Ma; Nishiizumi et al., 2007, Chmeleff et al., 2010; Korschinek et al., 2010). Based on results for other tektites, the concentrations of ^{10}Be were expected to be ~10^7 atom/g. Typical ^{10}Be concentrations of soils are higher, ~10^8 atom/g (c.f. Willenbring and von Blanckenburg, 2010). To remove possible surface contamination due to the presence of ^{10}Be in adhering soils or adsorbed from groundwater, the samples were etched in 4 mL of 1 M HF for 60 minutes (Serefiddin et al., 2007). After etching, the samples were washed with deionized water and dried. Etching losses, mostly 4–5 %, were larger for samples B11 and B12, 7% and 11%, respectively. Unlike the others, these two samples consisted not of one chip, but of several along with some powder. As a result, they presented larger specific surface areas to HF.

The preparation of ^{10}Be for accelerator mass spectrometry (AMS) required addition of ^9Be carrier, sample dissolution and equilibration with that carrier, and the chemical separation of Be from the solution as the oxide. To the sample masses used for these analyses, we added ~2 mg of Be in 1 mL of 10% (vol/vol) HNO_3, 4 mL of concentrated HF (49%), and 4 mL of concentrated $HClO_4$. The Be carrier solution (1041 ± 8 μg ^9Be/(g solution) in 5% HNO_3) was prepared at PRIME Lab from phenacites and has low $^{10}Be/^9Be$ ratio, typically $<10^{-15}$. The mixture was placed in a Teflon cup, packed into a Parr Bomb, and heated to 100 °C for about one week. The resulting solution was evaporated and taken up in 9 M HCl for anion exchange

(Dowex 1-X8 chloride form, 100–200 mesh). The eluates from anion exchange were evaporated and their residues dissolved in 1 M HCl. Then, the pH was adjusted to 7 in an ammonia-ammonium chloride buffer in order to precipitate beryllium as the hydroxide. After dissolution in 1 M HCl, beryllium was separated by cation exchange (Dowex 50Wx8 hydrogen form, 200–400 mesh) and purified by precipitation as described by Vogt and Herpers (1988).

2.7. Methods: Be-10 accelerator mass spectrometry

The $^{10}Be/^{9}Be$ ratios (atom/atom) of the samples were measured by accelerator mass spectrometry at Purdue University's PRIME Lab. These ratios are obtained through comparison with secondary standards that ultimately reference a primary standard for which the decay rate (activity) of ^{10}Be ($d^{10}Be/dt$), rather than the $^{10}Be/^{9}Be$ ratio, is accurately known (Nishiizumi et al., 2007). In effect, the $^{10}Be/^{9}Be$ ratios reported in this work are calculated from an equation of the form:

$$\left(\frac{^{10}Be}{^{9}Be}\right)_{Sample,Reported} = \frac{t_{1/2}(^{10}Be)}{Ln(2)}\left(\frac{d^{10}Be}{dt}\right)_{Std}\frac{\left(\frac{^{10}Be}{^{9}Be}\right)_{Sample,Measured}}{\left(\frac{^{10}Be}{^{9}Be}\right)_{Std,Measured}}$$

where the subscript 'Measured' refers to experimental data obtained by accelerator mass spectrometry after corrections for blank. We measured the $^{10}Be/^{9}Be$ of three procedural blanks and adopted the average, $^{10}Be/^{9}Be = (2.4 \pm 0.8) \times 10^{-15}$, in making corrections to the measured sample ratios. Typical $^{10}Be/^{9}Be$ ratios measured for the samples, $\sim 13 \times 10^{-15}$, were about five times larger than the average blank. Inspection of this equation shows that the $^{10}Be/^{9}Be$ ratios reported depend linearly on the value adopted for the ^{10}Be half-life. In this work, we have used the half-life of 1.36 ± 0.07 Ma proposed by Nishiizumi et al. (2007). Notwithstanding its implications to the contrary, our earlier report (in an abstract) also used this value to obtain $^{10}Be/^{9}Be$ ratios. We choose the 1.36 Ma half-life to maintain consistency with a large body of recent ^{10}Be measurements made at PRIME Lab. Subsequent, independent studies have given a more precise and slightly higher value of 1.387 ± 0.012 Ma for the ^{10}Be half-life (Chmeleff et al., 2010; Korschinek et al., 2010). Interested readers can re-normalize the $^{10}Be/^{9}Be$ ratios reported below (see results section) to this scale by multiplying by 1.387/1.36 [Ma/Ma]; the differences, ~2%, are well within the uncertainties of the measurements and negligible for the purposes of the discussion here.

Our earlier measurements of $^{10}Be/^{9}Be$ ratios in tektites (Ma et al., 2004; Serefiddin et al., 2007), also made at PRIME Lab, incorporated what was then the best estimate of the ^{10}Be half-life, 1.5 Ma. To compare the older $^{10}Be/^{9}Be$ ratios of tektites with the new ones for the Belize glasses, we multiplied the older results by a factor of 1.36/1.5 [Ma/Ma].

3. RESULTS

3.1. Petrography

In transmitted light, the glass has a yellow brown to brown color, but most of the specimens contain lighter and/or darker patches, bands, or schlieren (see Table 2 for a detailed description; Fig. 2). In half of the specimens the light colored bands/streaks are parallel or subparallel to the long axis. The lighter areas often have lower abundances of vesicles and lechatelierite than the predominant matrix glass, whereas the darker patches, bands, and streaks generally have higher concentrations of vesicles and lechatelierite particles.

Vesicles and lechatelierite are present in all the specimens. The vesicles exhibit a wide range in abundance (Fig. 2a,b) and size from one specimen to another (Table 2). For example, based on point counts, the abundance ranges from 0.1 up to 8.4 vol.% and the maximum diameter in the specimens ranges between 185 and 1200 μm. The vesicles are spherical in all the specimens except one (B18). In B18, most of the vesicles are slightly oval in shape and sometimes slightly irregular.

The lechatelierite particles range from equant, to elongate, to long and sinuous in shape (e.g., see Fig. 2), but most are elongate in shape. Most lechatelierite particles have vesicles associated with them (they are mostly in the tektite glass, but in contact with the lechatelierite particle). Like the vesicles, the lechatelierite particles vary in abundance and size from one specimen to another (Table 2). The maximum size ranges from ~130 × 340 μm (in B16) up to ~800 × 1700 μm (in B3; see Fig. 2c). The equivalent size (i.e., diameter) in equant grains (all three axes the same length) would be between 200 and 1100 μm, which is fine to coarse sand size. The lechatelierite particles are usually irregular in shape. Assuming that the original quartz grains from which they were formed by melting were more or less equant in shape, the original size can be estimated by taking an average of the three dimensions (length, width, and depth). The length and width can be measured, but depth has to be estimated. The average of the three dimensions is an estimate of the size of the equidimensional quartz grain and can be used to indicate the size distribution, which gives information about the type of sediment/rock; i.e., shale siltstone, fine sandstone, etc.). However, most of the lechatelierite particles are fine sand size or smaller. The above data indicate that the source sediment/rock was mostly silt to fine sand size, with a coarser component (at least in terms of the quartz component). Nonetheless, an unknown amount of finer quartz grains was probably melted and mixed in with the other melt to make the glass.

A few lechatelierite particles in some specimens (B4, B9, B15, B18) contain dark opaque to brown translucent regions (e.g., Fig. 2e,f). An attempt to recover one of these grains in order to identify the dark opaque region was not successful.

There are two transparent, colorless inclusions with lower relief than lechatelierite in specimen B18. The lower relief indicates that they have a refractive index (R.I.) close to that of the tektite glass, which, based on the composition probably has a R.I. of ~1.54. This is close to the R.I. of quartz; however, these inclusions are not birefringent. One is equant and contains a large opaque dark to translucent brown region (Fig. 2g). This inclusion also contains a small (~15 × 29 μm) grain with high relief and a shape similar to a zircon. The other inclusion is an equant grain

Table 2
Petrography of Belize tektites.

Sample number	Color[1]	Schlieren[1]	Glass vol. %	Vesicles		Lechatelierite		Mineral grains	Dia. of largest vesicle[3] (μm)
				Abundance[2]	Vol. %	Abundance[2]	Vol. %		
B1	BrY	No	99.9	Rare	0.1	Rare	<0.1	No	185
B2	YBr	Yes (pYBr)	99.8	Common to abundant	0.2	Rare to common	<0.1	No	380
B3	BrY	No	99.9	Rare to common	0.1	Common	<0.1	No	940
B4	YBr	Yes (drkBr)	96.5	Common to abundant	3.3	Common to abundant	0.2	No	450
B5	YBr	No	99.2	Common to abundant	0.8	Rare to common	<0.1	No	620
B6	YBr	Yes (pYBr)	99.3	Common to abundant	0.7	Rare to common	<0.1	No	650
B7	YBr	Yes (BrY)	99.8	Common to abundant	0.2	Common	<0.1	No	350
B8	YBr	Yes (drkBr & pBrY)	97.6	Common to abundant	2.4	Rare to common	<0.1	No	565
B9	YBr	Yes (drkBr & pBrY)	99.7	Common	0.3	Rare to common	<0.1	No	955
B10	YBr	Yes (BrY at one end)	99.4	Common to abundant	0.6	Rare to common	<0.1	No	450
B11	YBr	Yes (faint BrY)	99.1	Common	0.9	Rare to common	<0.1	No	530
B12	YBr	Yes (a short BrY streak)	99.7	Common	0.3	Rare to common	<0.1	Yes?	490
B13	YBr	No	91.6	Common to abundant	8.4	Rare to common	<0.1	No	1200
B14	YBr	Yes (drkBr)	99.7	Common	0.3	Rare to common	<0.1	No	350
B15	YBr	Yes (drkBr streaks & patches)	99.5	Common to abundant	0.3	Common to abundant	0.2	No	420
B16	YBr	Yes (drkBr near one edge)	99.3	Common to abundant	0.7	Rare to common	<0.1	No?	470
B17	YBr	Yes (a drkBr stripe)	98.4	Common to abundant	1.6	Rare to common	<0.1	No	600
B18	YBr	Yes (drkBr streaks)	98.0	Abundant	1.6	Common to abundant	0.4	Yes	330

[1] YBr = yellowish brown, BrY = brownish yellow, Br = brown; drk = dark, p = pale, Y = yellow.
[2] Abundances are based on 1000 point counts. Where a range in abundance is given, if one is underlined, then it is closer to the estimated abundance; e.g., common to abundant means the abundance is closer to common than to abundant.
[3] Maximum vesicle diameter is the average diameter of the long and short axes for an elongated spherule.

(170 × 200 μm) with an opaque interior (120 × 130 μm) having a dark toasted appearance in transmitted light (Fig. 2h), but in reflected light it is opaque bluish white. The transparent outer rim of the inclusion is isotropic. A few small transparent grains in the transparent region have higher relief and higher refractive index than the rest of the transparent part of the grain. The opaque interior may be microcrystalline. An inclusion in B9 has a ballen-like texture (Fig. 2e) and contains dark opaque region. Under crossed polarizers, the grain appears to be weakly birefringent with a mosaic texture, the mosaic-like texture and the weak birefringence may be due numerous bubbles in or adjacent to the inclusion. Three grains (crystals?) with high relief and low birefringence were observed in the particle. The largest is ~30 × 75 μm in size. These grains remain unidentified.

3.2. Geochemistry

All glasses show a high internal (within each thin section) and external (between the different glass samples) homogeneity for all analyzed major elements, as determined by electron microprobe analyses. In terms of internal homogeneity only two samples (B4 and B10) show areas of different composition, with SiO_2 – rich regions with concentrations between 70.16 and 99.67 wt%. All other glasses show values between 59.27 and 66.89 wt% SiO_2. This is also evident from the backscattered-electron images shown in Fig. 3. A high degree of homogeneity between the samples is apparent for SiO_2, Al_2O_3 and FeO. The variation is largest for the K_2O content. The Mg-number varies between 19.7 and 24.3.

Variations in major element composition for Belize glasses are illustrated in the total alkali-silica diagram (Fig. 4). All Belize glasses are subalkaline, and of andesitic to dacitic composition. They fit well the pattern of Central American Arc samples of similar SiO_2 content (e.g., Alves et al., 2002). Compared to the samples of the four major tektite strewn fields, they show significantly higher alkali and lower silica content. Average Belize glass data from Rochette et al. (2021) fit well with our data, whereas Pantasma crater data (Rochette et al., 2019) are more widely scattered.

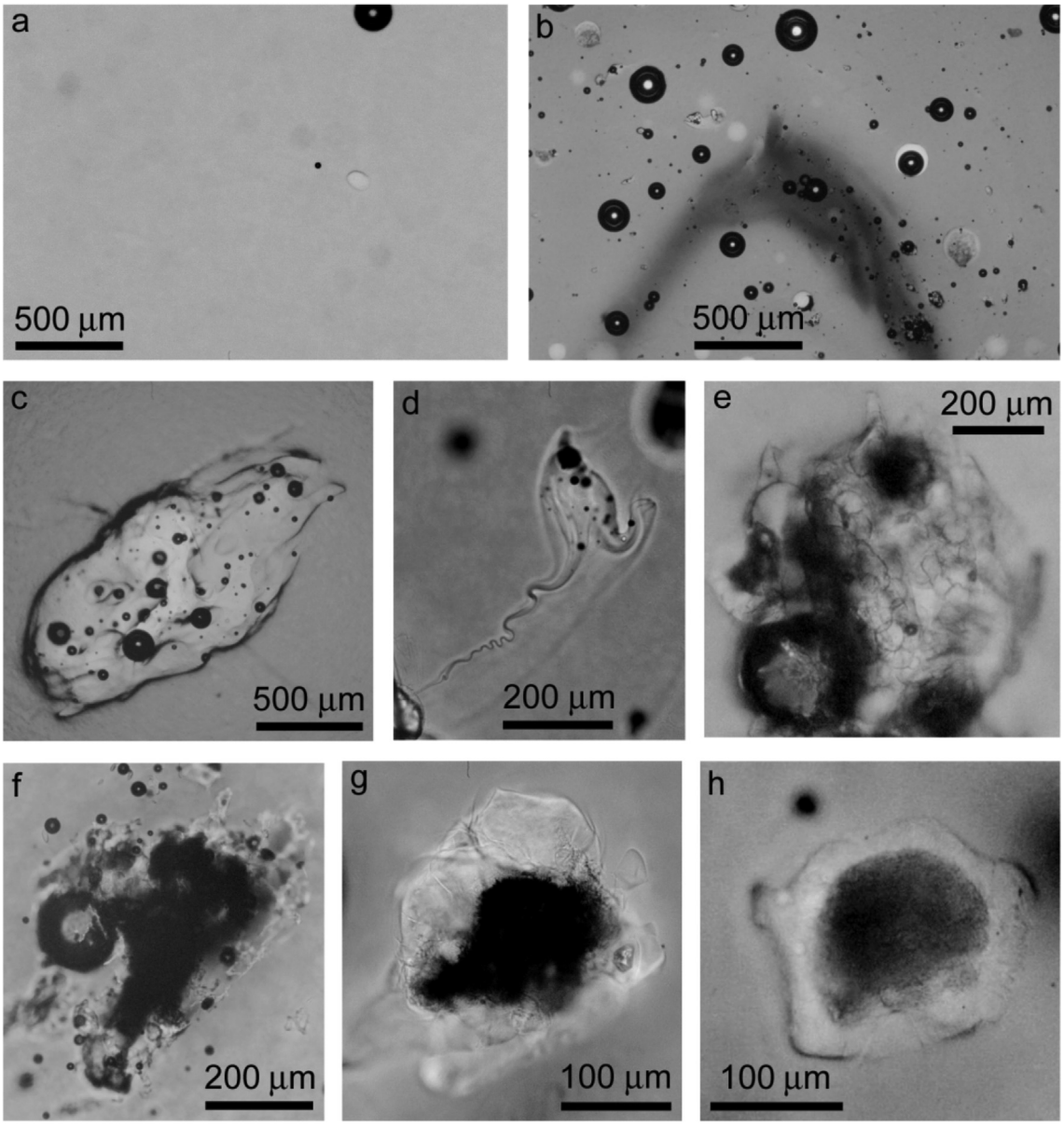

Fig. 2. Photomicrographs of sections of Belize tektites taken in transmitted light. The specimens shown in (a) and (b) illustrate variations between samples. Both images cover approximately the same area at the same magnification. (a) This specimen (B1) has a low abundance of lechatelierite and vesicles. Two spherical vesicles and one ~100 µm long lechatelierite particle (light color) are present. No schlieren are present. (b) In contrast to B1 (a), this specimen (B4) contains abundant spherical vesicles and lechatelierite particles. A dark brown chevron-shaped schlieren is also present. (c) A large (~0.8 × 1.7 mm) lechatelierite particle in specimen B3. Note the large number of vesicles associated with the lechatelierite. (d) An irregular shaped lechatelierite particle with a long (~400 µm) sinuous tail in specimen B16. Several spherical vesicles are associated with the main mass of the particle. Some faint schlieren run diagonally across the field of view approximately parallel to the tail. (e) Part of a lechatelierite particle with ballen-like texture in specimen B9. There are a few dark opaque to translucent brown regions within the particle and a few vesicles associated with it. The largest vesicle (lower left corner) is ~300 µm in diameter and appears to be somewhat irregular. (f) Remnants of a lechatelierite particle with a large dark opaque to translucent brown region in specimen B4. Numerous spherical vesicles (up to 150 µm in diameter) are associated with the lechatelierite. (g) An approximate equant transparent colorless inclusion with a large central dark opaque to translucent brown region in B18. This inclusion has a lower relief than the lechatelierite particles. Note the lack of any vesicles associated with this inclusion. On the right side of the inclusion is a smaller grain (~15 × 29 µm) with high relief and a shape similar to that of a zircon. (h) This is a most unusual inclusion also in specimen B18. It is transparent colorless with a large translucent dark brown central region; however, in reflective light the central region is opaque bluish white. The grain has a very faint ballen-like texture (probably not visible at the scale of the photomicrograph).

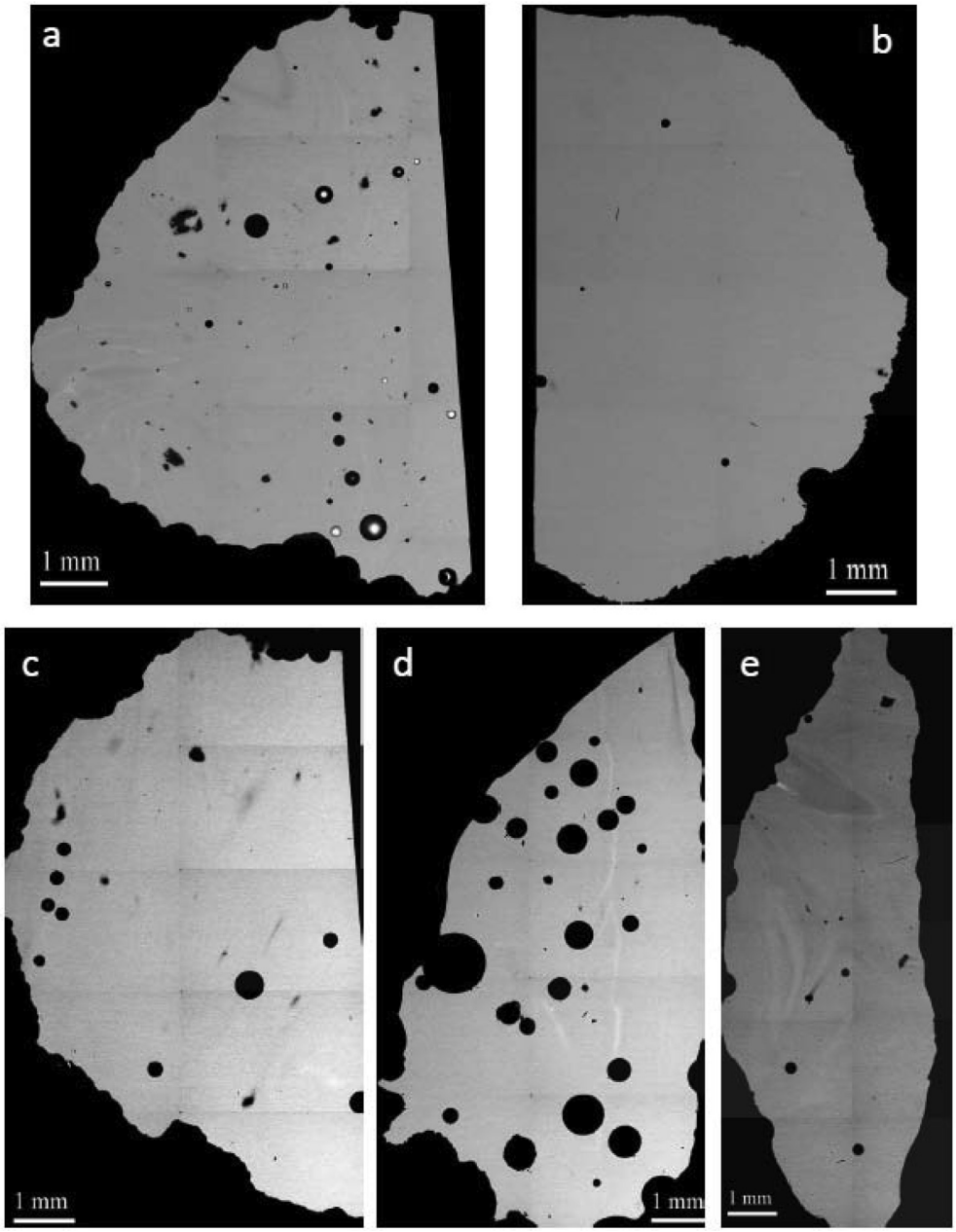

Fig. 3. Back-scattered electron images of selected Belize glass samples, showing relatively homogeneous composition (except a few schlieren and (dark) lechatelierite inclusions) and the presence of vesicles: (a) sample B4, (b) sample B5, (c) sample B10, (d) sample B13, and (e) sample B16.

Trace element compositions of the Belize glass samples analyzed in this study are compiled in Table 3. Mantle-normalized trace element patterns are shown in Fig. 5. Like the major elements they closely trend Central American Arc samples, with the exception of two samples that show variations from the overall trend. Sample B2 displays an inverse HREE pattern and, e.g., sample B16 is slightly enriched in Sr and Ba.

Chromium, cobalt, and nickel abundances (Table 3) of Belize glass samples (B1-B18) are roughly positively correlated and range from ~23 to ~49 ppm, from ~10 to ~15 ppm and from ~60 to ~150 ppm, respectively. Interelement ratios vary between 1.7 and 3.8 for Ni/Cr and between 2.0 and 2.5 for Cr/Co. These values are comparable to concentrations and interelement ratios reported from subduction-related lavas from the Central American Arc (e.g., Alves et al., 2002), although the latter span a wider range.

The $^{87}Sr/^{86}Sr$ and $^{143}Nd/^{144}Nd$ isotope data, as well as associated Sr and Nd concentrations, are given in Table 4. The Belize glasses are extremely homogeneous in their $^{143}Nd/^{144}Nd$ ratio. The measured values vary between 0.512825 and 0.512835. For $^{87}Sr/^{86}Sr$, the variations are slightly greater, with values ranging from 0.703951 to

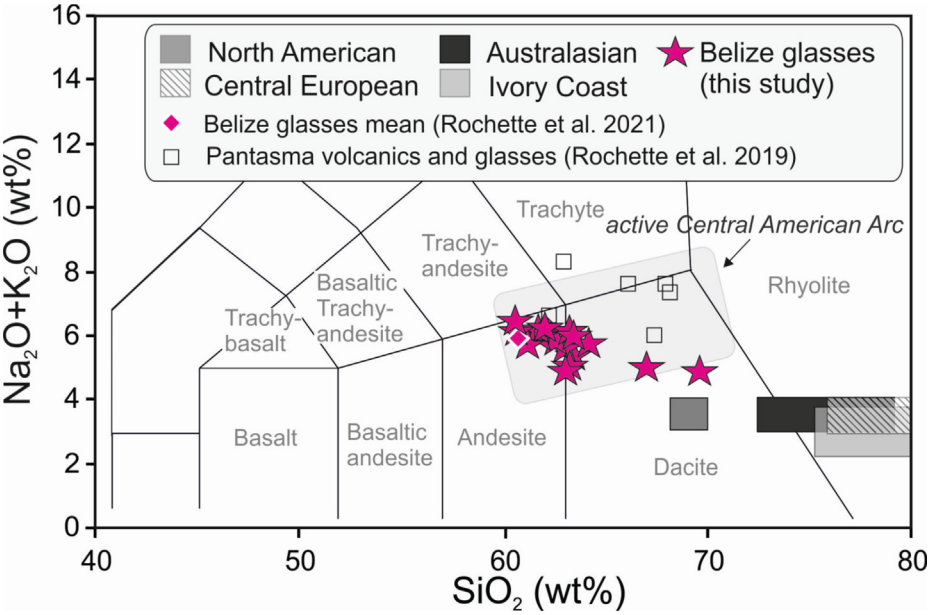

Fig. 4. Chemical classification diagram of volcanic rocks (according to Le Maitre et al. 1989) showing the Belize glasses in relation to the tektites from other strewn fields and selected samples of the Central American Arc of similar SiO_2 content. Data for the tektite strewn fields are from Shaw and Wasserburg (1982) and for the Central American Arc from Carr et al. (2003); comparison data for Belize glasses and Pantasma volcanics and glasses from Rochette et al. (2019, 2021).

0.704081 (note: as the samples are young (~800 ka), a back calculation to initial values is not necessary in the Sr- and Nd-systems). These data are in good agreement with those given by Rochette et al. (2021) for other Belize samples, as well as with selected magmatic rocks of the Central American Arc, in particular from Honduras and Guatemala (Patino et al., 1997, 2000; Walker et al., 2000, 2001; Carr et al., 1990, 2003). Compared to impact-related glasses, from the four major strewn fields as well as the Zhamanshin impact structure, the Haiti and DSDP 612 glasses, and Libyan Desert Glass (Fig. 6) the Belize glasses have a clear mantle affinity. Data by Rochette et al. (2021) for Belize glasses are almost identical to our data. Figures 7 and 8 provide additional geochemical aspects of these glasses (see below).

Concentrations of the HSEs and $^{187}Os/^{188}Os$ ratios of five Belize glasses (B02, B04, B05, B06 and B07) are summarized in Table 5. Concentrations of HSEs range from 0.169 to 1.946 ppb for Re, 0.035 to 0.145 ppb for Ir, 0.001 to 0.005 ppb for Os and 1.197 to 26.94 ppb for Pt. Whereas Os concentrations are extremely low compared to the average upper continental crust (UCC = ~31 ppt Os; Peucker-Ehrenbrink and Jahn 2001), Ir concentrations in Belize glasses are either comparable (e.g., B06) to those in the upper continental crust (UCC = ~22 ppt Ir; Peucker-Ehrenbrink and Jahn 2001), or have higher contents. In all analyzed Belize glasses, except for sample B06, the Re concentrations are comparable to those of the UCC, but Pt concentrations are significantly higher (UCC = ~198 ppt Re and 510 ppt Pt; Peucker-Ehrenbrink and Jahn 2001). Corresponding interelement ratios in the Belize glasses range from 0.014 to 0.029 for Os/Ir and from 8.26 (sample B05) to 626.6 for Pt/Ir ratios (UCC = ~1.4 Os/Ir and ~23.2 Pt/Ir; CI chondrites = 1.06 Os/Ir and 2.03 Pt/Ir; Tagle and Berlin 2008).

The $^{187}Os/^{188}Os$ isotope ratios in the Belize glasses are ~0.135 for sample B05, ~0.2487 for sample B02, ~0.3316 for sample B04, ~0.337 for sample B06, and 1.322 for sample B07. Replicate measurements (of unspiked samples) were undertaken for four of these samples (B02, B05, B06, and B07) and yield, within analytical uncertainty, indistinguishable $^{187}Os/^{188}Os$ ratios (see Table 5). The measured $^{187}Os/^{188}Os$ ratios in Belize glasses range from near-chondritic values (sample B05) to typical crustal values (UCC = ~1.05; Peucker-Ehrenbrink and Jahn, 2001). Due to Os abundances in the analyzed samples being in the very low ppt range, and Re concentrations up to a low ppb level, corresponding $^{187}Re/^{188}Os$ ratios in the analyzed samples are exceptionally high and range from ~869 to ~9354.

There are no literature values for Os abundances and isotopes for subduction-related volcanics from the active Central American Arc, which does not allow a direct comparison between the local mantle and the Belize glasses. The Re and Os concentrations and corresponding interelement ratios from the Belize glasses are comparable to those from arc localities world-wide (e.g., Alves et al., 2002). Figure 9 provides a summary of the Os systematics of Belize glasses and arc magmas, along with comparisons to Ivory Coast tektites and the upper continental crust.

3.3. Iron oxidation state and water content

Experimental Fe K-edge XANES spectra are shown in Fig. 10: The shape and edge energy position of the Belize tektite spectra are very similar to those of splash form tek-

Table 3
Major and trace element composition of the 18 Belize tektite samples.

Sample	B1 (n = 12)	B2 (n = 12)	B3 (n = 12)	B4 (n = 22)	B5 (n = 15)	B6 (n = 29)	B7 (n = 12)	B8 (n = 15)	B9 (n = 15)	B10 (n = 18)	B11 (n = 14)	B12 (n = 10)	B13 (n = 17)	B14 (n = 17)	B15 (n = 16)	B16 (n = 20)	B17 (n = 20)	B18 (n = 15)
SiO_2	63.37	62.77	63.38	61.92	62.72	62.30	63.43	61.05	60.73	63.65	62.33	62.27	62.49	61.60	62.01	61.74	64.22	61.92
TiO_2	0.95	0.97	0.98	0.90	0.96	0.95	0.97	0.95	0.91	0.94	0.93	0.89	0.93	0.84	0.88	0.91	0.94	0.96
Al_2O_3	16.86	16.85	17.05	17.42	16.64	16.77	16.32	17.08	17.83	16.12	16.97	16.85	16.84	17.46	17.20	17.69	16.40	17.20
FeO	6.39	6.32	6.46	6.24	6.40	6.37	6.32	6.45	6.00	6.16	6.31	6.06	6.18	5.95	5.94	6.22	6.35	6.48
MnO	0.17	0.15	0.17	0.15	0.16	0.16	0.16	0.15	0.15	0.15	0.15	0.16	0.15	0.14	0.15	0.16	0.15	0.16
MgO	1.89	1.84	1.88	1.92	1.81	1.71	1.76	2.04	1.84	1.74	1.83	1.93	1.78	1.91	1.86	2.00	1.55	1.92
CaO	4.83	4.85	4.59	5.03	4.76	4.70	4.53	5.40	5.30	4.70	5.05	5.12	4.90	5.12	5.13	5.33	4.36	5.31
Na_2O	3.12	3.77	3.30	3.99	3.86	4.16	3.97	4.19	4.46	3.60	3.82	4.06	4.01	4.04	4.16	4.03	3.57	4.08
K_2O	1.68	1.89	1.74	1.87	1.93	2.11	2.05	1.86	2.02	1.92	1.88	1.87	1.97	1.79	1.84	1.77	2.21	1.91
Total	99.25	99.42	99.54	99.45	99.25	99.23	99.50	99.16	99.24	98.98	99.26	99.23	99.25	98.84	99.15	99.85	99.76	99.93
Sc	20.8	17.5	20.7	19.9	19.7	18.9	21.1	19.4	20.5	19.9	18.8	19.6	18.9	17	20.6	19.6	20.5	19.6
Cr	41.5	31.4	30.5	33.7	35.7	22.7	28.6	29.8	41.9	43.6	26.2	41.6	30.3	32.2	48.7	39.3	27.4	33.5
Co	12.0	11.2	11.8	13.7	12.8	10.2	14.2	13.5	15.1	12.8	11.7	14.2	12.3	12.2	15.2	15.5	11	12.8
Ni	70.0	80.9	72.4	91.9	76.3	60.1	88.1	74.2	116.6	80.1	58.7	84.8	89.4	67.1	131.4	149.9	59.3	73.0
Zn	34.6	17.0	36.5	45.5	33.8	56.5	32.8	61.4	48.6	35.7	39.3	36.9	48.4	40.6	29.8	48.6	42.0	67.8
Ga	1.69	2.89	7.73	10.41	4.83	3.67	11.20	6.95	1.65	2.21	4.73	3.35	4.73	2.53	3.07	8.75	5.40	5.01
As	<2.3	<2.1	<2.3	<2.4	<2.4	<1.7	0.62	<2.7	<3.0	<1.9	<2.2	<2.6	<2.2	<2.1	<2.8	<1.0	<2.3	<2.3
Se	<2.2	<0.6	<1.5	<1.5	<1.8	<1.5	<2.0	<1.6	<2.6	<1.4	<1.8	<2.0	<1.7	<1.6	<1.4	<1.8	<1.9	<1.7
Br	<2.0	<1.9	<1.5	<1.6	<1.9	<1.3	<0.6	<1.8	<2.7	<1.7	<1.6	<2	<1.7	<1.5	<2.2	<1.9	<1.7	<1.8
Rb	35.6	37.6	36.4	39.7	43.8	42.4	46.1	37.3	49.4	42.2	40.4	34.7	43.6	35.1	45.0	48.0	39.3	43.6
Sr	280	256	288	271	277	283	266	267	288	242	273	265	265	283	362	356	229	282
Zr	213	205	239	213	230	229	230	204	295	257	225	217	234	218	263	261	242	245
Sb	<0.6	<0.6	<0.3	0.1	<0.5	<0.3	<1.1	<0.4	<0.8	<0.5	<0.4	<0.5	<0.4	<0.4	<0.6	<0.2	<0.4	<0.4
Cs	1.34	0.75	1.41	1.25	1.30	1.15	1.45	1.30	1.51	1.27	1.07	1.32	1.36	1.20	1.49	1.51	0.87	1.36
Ba	375	458	400	372	356	338	410	323	451	328	359	337	373	328	442	432	372	385
La	21.1	22.8	20.5	19.1	19.5	19.1	21.3	18.1	20.8	20.0	19.6	17.8	20.3	17.4	20.8	20.5	20.4	19.0
Ce	42.2	35.3	41.2	37.6	39.7	38.2	43.7	35.5	41.2	40.1	37.5	34.5	38.5	34.4	42.2	39.6	41.1	38.7
Nd	21.5	26	24.6	21.6	23.2	21.1	25.1	19.2	24.4	22.0	19.9	20.3	22.6	19.5	22.7	23	22.6	22.8
Sm	6.14	7.29	6.47	5.78	6.01	5.59	6.26	5.23	6.44	5.79	5.60	5.54	6.11	4.87	6.38	6.42	6.21	5.92
Eu	1.86	0.94	1.78	1.61	1.69	1.66	1.82	1.51	1.78	1.76	1.63	1.53	1.61	1.51	1.79	1.73	1.80	1.65
Gd	5.74	3.31	6.26	5.16	5.73	5.49	6.25	5.17	7.16	6.46	5.16	5.67	5.26	4.91	5.72	5.87	5.66	5.72
Tb	1.12	0.61	1.07	0.96	1.00	0.96	1.12	0.88	1.16	1.01	0.93	0.90	0.98	0.84	1.09	1.11	1.05	0.96
Tm	0.63	0.51	0.6	0.53	0.59	0.52	0.51	0.52	0.46	0.57	0.51	0.5	0.54	0.46	0.61	0.63	0.59	0.53
Yb	3.87	4.35	3.77	3.46	3.54	3.34	3.83	3.19	3.19	3.50	3.39	3.13	3.46	2.89	3.65	3.52	3.92	3.41
Lu	0.59	0.7	0.61	0.54	0.58	0.55	0.63	0.5	0.58	0.56	0.54	0.5	0.56	0.48	0.60	0.56	0.6	0.55
Hf	4.95	4.58	4.85	4.47	4.6	4.41	4.84	4.09	4.59	4.50	4.33	4.04	4.53	3.96	4.85	4.69	4.89	4.54
Ta	0.46	0.27	0.46	0.39	0.43	0.39	0.42	0.36	0.46	0.42	0.37	0.39	0.43	0.31	0.50	0.5	0.44	0.44
W	<8.9	<8.1	<10	<11	<10	<7.2	<4.3	<12	<12	<7.4	<9.2	<11	<9.2	<8.7	<11	<9.8	<9.1	<9.6
Ir (ppb)	<2.4	<0.6	<1.6	<1.6	<2	<1.6	<1.6	<1.6	<2.9	<1.6	<1.9	<2.3	<1.8	<1.7	<1.6	<1.9	<2.0	<1.7
Au (ppb)	<5.8	23	<3.0	<3.1	<4.6	<2.8	<1.9	<3.4	<7.7	<5.0	<3.8	<4.8	<3.9	31	<5.4	<3.7	<4.1	<4.0
Th	4.23	3.63	4.16	3.78	3.96	3.68	3.67	3.46	4.31	3.84	3.65	3.51	3.86	3.3	4.26	4.26	4.05	3.86

(*continued on next page*)

Table 1 (*continued*)

Sample	B1 (n = 12)	B2 (n = 12)	B3 (n = 12)	B4 (n = 22)	B5 (n = 15)	B6 (n = 29)	B7 (n = 12)	B8 (n = 15)	B9 (n = 15)	B10 (n = 18)	B11 (n = 14)	B12 (n = 10)	B13 (n = 17)	B14 (n = 17)	B15 (n = 16)	B16 (n = 20)	B17 (n = 20)	B18 (n = 15)
U	<2.1	<2.1	0.87	1.18	0.65	0.79	0.9	1.12	<2.9	<1.8	1.30	1.04	0.97	1.06	1.37	1.25	0.84	1.06
Mg #	22.8	22.6	22.6	23.5	22.0	21.2	21.8	24.0	23.4	22.0	22.5	24.2	22.4	24.3	23.8	24.3	19.7	22.9
Ni/Cr	1.69	2.57	2.37	2.73	2.14	2.65	3.07	2.49	2.78	1.84	2.24	2.04	2.95	2.09	2.70	3.81	2.17	2.18
Cr/Co	3.45	2.81	2.58	2.47	2.78	2.23	2.01	2.21	2.78	3.41	2.23	2.93	2.46	2.64	3.20	2.53	2.49	2.62
Ba/La	17.81	20.11	19.45	19.46	18.23	17.66	19.28	17.81	21.64	16.40	18.28	18.97	18.38	18.85	21.24	21.06	18.19	20.20
U/Th	nd	nd	0.21	0.31	0.16	0.21	0.25	0.32	nd	nd	0.36	0.30	0.25	0.32	0.32	0.29	0.21	0.27

Major elements in wt%, trace elements in ppm (exception as noted). All Fe is given as FeO. Major elements measured by EMP, trace elements by INAA (see text). For major elements an average value is given for single glass samples. (n) gives the number of point measurements included. All EMP measurements are given in the appendix. nd = not defined.

tites from all four known strewn fields studied previously (Giuli et al., 2002, 2010a,b), suggesting the presence of predominantly divalent Fe. Moreover, the pre-edge peak has a shape and centroid energy similar to those of tektites from the North American, Central European, Ivory Coast, and Australasian strewn fields (Giuli et al., 2002, 2010a,b).

The pre-edge peak is related to an *s-d* like electronic transition. The *s-d* transition is dipole-forbidden ($\Delta\ell\neq1$), but can become partially allowed by mixing of the Fe *d*-states with the *p*-states of the surrounding oxygen atoms. This means that the pre-edge peak energy position and intensity depend strongly on both the atomic geometry around Fe and on the mean Fe oxidation state (Calas and Petiau, 1983; Brown et al., 1995). Accurate evaluation of the pre-edge peak centroid energy and integrated area and comparison with those of Fe model compounds can provide quantitative information on both Fe oxidation state and coordination environment (see Calas and Petiau, 1983; Brown et al., 1995; Wilke et al., 2001; Farges, 2001; Giuli et al., 2002, 2011): its intensity will be almost zero in case of regular octahedral symmetry (O_h) around the absorber, whereas it will reach its maximum in the case of tetrahedral symmetry (T_d).The background-corrected pre-edge peaks of the Belize tektites Fe- XANES spectra are shown in Fig. 11 (a-c), along with the pseudo-Voigt components used in the fitting procedure and their sums. Each pre-edge peak can be fitted with two to three components whose energies (ca. 7112.6, 7113.9–7114.3, and 7114.5–7115.3 eV) are consistent with those of divalent and trivalent Fe model compounds (e.g., Giuli et al., 2002). In particular, while the first and last components can be ascribed to contributions from Fe^{2+} and Fe^{3+} respectively, the component at intermediate energy results from contributions by both Fe^{2+} and Fe^{3+}. The integrated area of the pre-edge peaks vs. their centroid energies is plotted in Fig. 12 along with the data for Fe model compounds analyzed here and by others (Wilke et al., 2001; Farges, 2001; Giuli et al., 2002, 2008). For the sake of simplicity, the relative energy is plotted, where 0 is taken as the first maximum of the first derivative of metallic Fe spectrum. We take this approach to avoid confusion when comparing data with literature data where energies may be given on a scale for which a different edge energy of metallic Fe has been chosen. All model Fe(II) compounds plot at energies close to 0.9 eV above the metallic Fe edge, whereas Fe(III) model compounds plot at energies close to 2.4 eV.

The Belize tektite data plot within a narrow region close in energy to that of divalent Fe model compounds, meaning that most of the Fe is divalent. A mixing line (dotted line with small diamonds) has been calculated so as to connect:

(i) a pre-edge peak with a centroid at 0.9 eV above the edge of metallic iron and an integrated area intermediate to that of $^{[4]}Fe^{2+}$ and $^{[5]}Fe^{2+}$ model compounds ([4] and [5] indicate 4- and 5- coordinated iron);
(ii) a pre-edge peak with a centroid at 2.4 eV above the edge of metallic iron and integrated area intermediate to that of $^{[4]}Fe^{3+}$ and $^{[5]}Fe^{3+}$ model compounds.

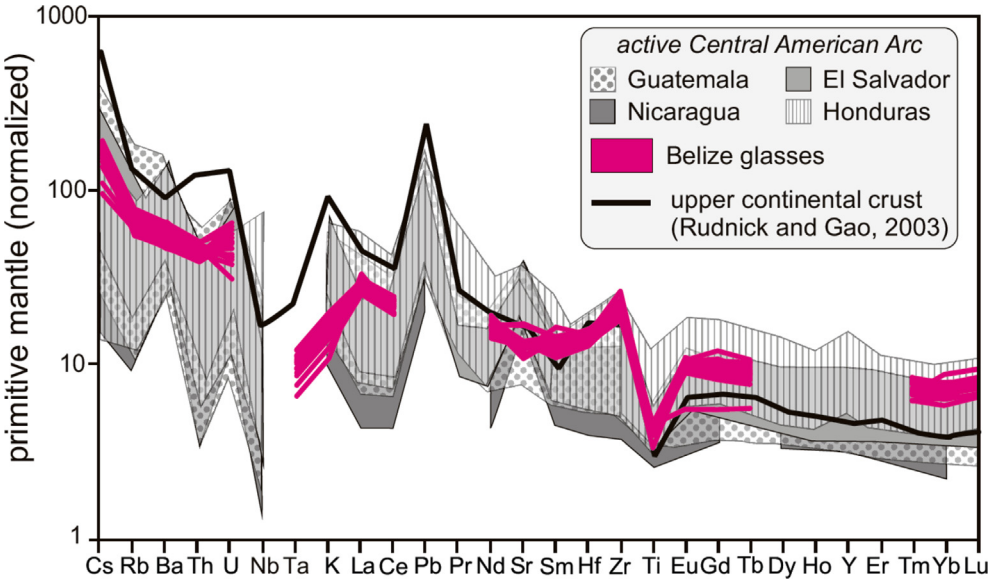

Fig. 5. Primitive mantle-normalized (following Sun and McDonough 1989) trace-element patterns for Belize glasses in comparison to Central American Arc samples (Carr and Pontier, 1981; Carr and Walker, 1987; Carr et al., 1990, 2003; Patino et al., 1997, 2000; Walker et al., 2000, 2001) and average Upper Continental Crust (Rudnick and Gao, 2003).

Table 4
Strontium and Nd concentrations and isotope compositions of selected Belize tektites. Strontium and Nd concentrations are from the INAA data set.

Sample	Sr (ppm)	$^{87}Sr/^{86}Sr$	2σ	εSr	Nd (ppm)	$^{143}Nd/^{144}Nd$	2σ	εNd
B01	280	0.704008	± 3	−7.0	21.50	0.512830	± 4	3.7
B02	256	0.704041	± 3	−6.5	25.99	0.512830	± 4	3.7
B03	288	0.703980	± 4	−7.4	24.62	0.512830	± 3	3.7
B04	271	0.703995	± 4	−7.2	21.58	0.512828	± 3	3.7
B05	277	0.704033	± 4	−6.6	23.16	0.512828	± 3	3.7
B06	283	0.704081	± 3	−5.9	21.13	0.512829	± 3	3.7
B07	266	0.704061	± 4	−6.2	25.06	0.512825	± 3	3.7
B08	267	0.704030	± 4	−6.7	19.20	0.512832	± 3	3.8
B09	288	0.703984	± 3	−7.3	24.41	0.512830	± 3	3.7
B10	242	0.704035	± 4	−6.6	22.02	0.512834	± 4	3.8
B11	273	0.704031	± 4	−6.7	19.90	0.512831	± 4	3.8
B12	265	0.703951	± 4	−7.8	20.30	0.512835	± 3	3.8

εNd values are based on $^{143}Nd/^{144}Nd = 0.512638$ for the Chondritic Uniform Reservoir and εSr is relative to the present day bulk earth composition of $^{87}Sr/^{86}Sr = 0.7045$.

Analysis of the experimental pre-edge peak data provided quantitative $Fe^{3+}/(Fe^{3+}+Fe^{2+})$ ratios of $\leq 0.14 \pm 0.05$ for all samples. Based on the precision of the energy (±0.03 eV), we estimate the error in the $Fe^{3+}/(Fe^{3+} + Fe^{2+})$ ratios to be within ± 0.05. These results are in keeping with known Fe oxidation states of tektites from the North American, Central European, Ivory Coast, and Australasian strewn fields as determined with a variety of techniques, including titration, EPR, Moessbauer, and X-ray Absorption Spectroscopy (Fudali et al., 1987, Dunlap et al., 1998; Rossano et al., 1999; Giuli et al., 2002; Dunlap and Sibley, 2004; Giuli et al., 2010a,b).

The micro-FTIR spectra display an absorption band with a maximum at 3600 cm^{-1}, which is related to the total water content of the sample and whose intensity can be used to quantify the water content variation. The frequency of the absorption band is consistent with that already reported by Koeberl and Beran (1988), as are the asymmetry of the band and the full width at half maximum. The calculated water contents of selected spots are reported in Table 6 along with the chosen values of density (see "Methods" above).

The determined water contents of these tektites, listed in Table 6, range between 82 and 133 ppm and are in excellent agreement with those of tektites from other strewn fields reported in the literature (Beran and Koeberl, 1997, Koeberl and Beran, 1988, Giuli et al., 2013). In Fig. 13, the water contents are plotted as a function of the Fe redox

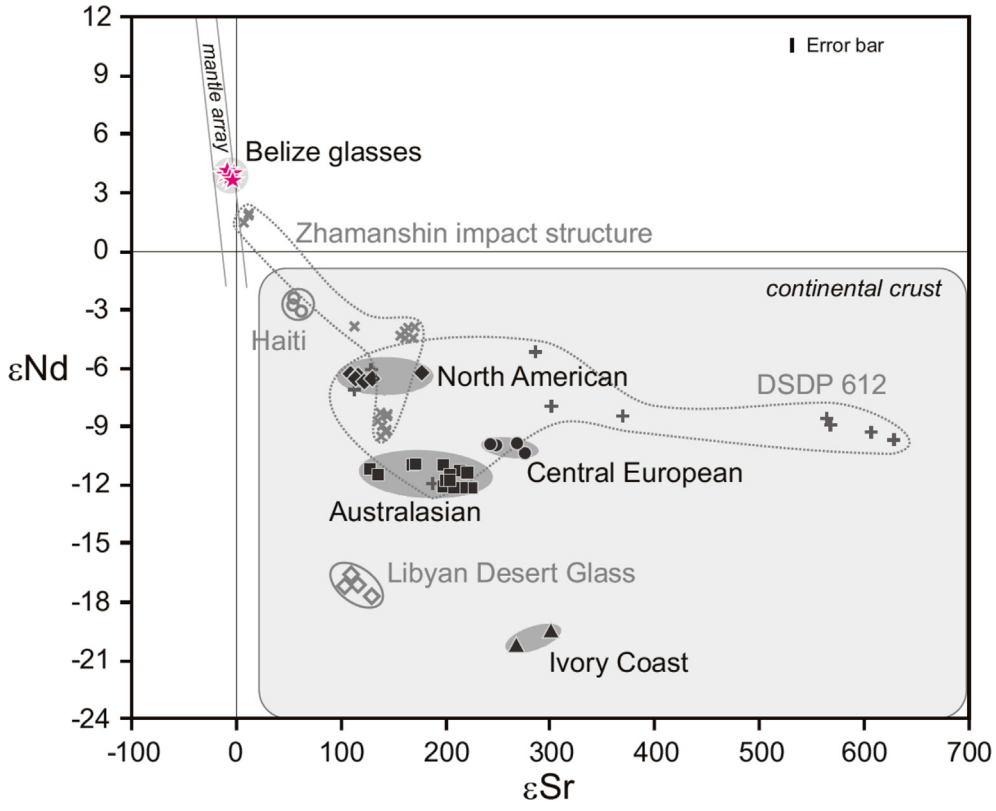

Fig. 6. Present-day εNd ratios plotted versus εSr ratios of Belize samples in relation to the tektite strewn fields (Shaw and Wasserburg, 1982; Ngo et al., 1985) and other impact related glasses from Haiti (Premo and Izett, 1992), the Libyan Desert (Barrat et al., 1997), the Zhamanshin impact structure (Ostermann et al., 1996; Shaw and Wasserburg, 1982; Schulz et al., 2020) and DSDP 612 (Stecher et al., 1989). Normalization: UR (Uniform Reservoir) for Sr and CHUR (Chondritic Uniform Reservoir) for Nd isotopic ratios, following Shaw and Wasserburg (1982).

ratio determined on the same samples: Water content shows no relation with the Fe redox ratio.

3.4. Be-10 measurements

The measured ^{10}Be concentrations (10^6 atom/g) of the seven samples analyzed ranged from 7 to 23 with an average of 12 ± 5, which, when decay-corrected for an ^{40}Ar/^{39}Ar age of 755 ka corresponds to 17 ± 7. Rochette et al. (2021) recently reported ^{10}Be contents between 4.4 and 8.2 in six Belize glasses (mean, 5.9 ± 1.4; mean at time of fall, 9.1 ± 2.1).

The mean ^{10}Be content of the Belize glasses is about $8 \times$ lower than the average of 100×10^6 atom/g measured for 100 Australasian tektites, corrected for an age of ~0.8 Ma (Ma et al., 2004; Schwarz et al., 2016; Jourdan et al., 2019). Fig. 14 shows our data for the ^{10}Be concentrations of Belize tektites, together with those for other tektites of Australasian tektites (Ma et al., 2004), Ivory Coast (Serefiddin et al., 2007) and the Belize dataset of Rochette et al. (2021). Because the published data of Australasian and Ivory Coast tektites used a ^{10}Be half-life of 1.5 Ma, we renormalized them to a ^{10}Be half-life of 1.36 Ma (Nishiizumi et al., 2007).

A difference between the Belize and Australasian samples is obvious. In Australasian tektites, regionally averaged ^{10}Be concentrations generally increase with increasing distance from Southeast Asia, the probable location of the tektite producing source region. Australian tektites lie up to ~8000 km from Southeast Asia and have the highest observed concentrations of ^{10}Be, $\sim 100 \times 10^6$ atom/g. Thus, if Belize glass and Australasian tektites had a common source, we would expect the ^{10}Be abundances in Belize glass, which are found at more than twice the distance of Australia from Southeast Asia, to be at least as large as those of the Australian tektites. In fact, the measured average for the Belize glasses is ten times smaller, $(12 \pm 5) \times 10^6$ atom/g, and does not show any relation to the Australasian strewn field. Based on the low abundance of ^{10}Be in the Belize glasses it seems most likely that they have a distinct geographical origin, i.e., do not belong to the Australasian strewn field. The internal variations of the Belize data (Table 7) could reflect the vertical position of the source material prior to impact, with sample B10 coming from a deeper and sample B11 from a shallower level.

The Belize glasses tend to have lower ^{10}Be contents than the Ivory Coast tektites. Correction of the group means to the respective times of fall (0.804 Ma for Belize glasses

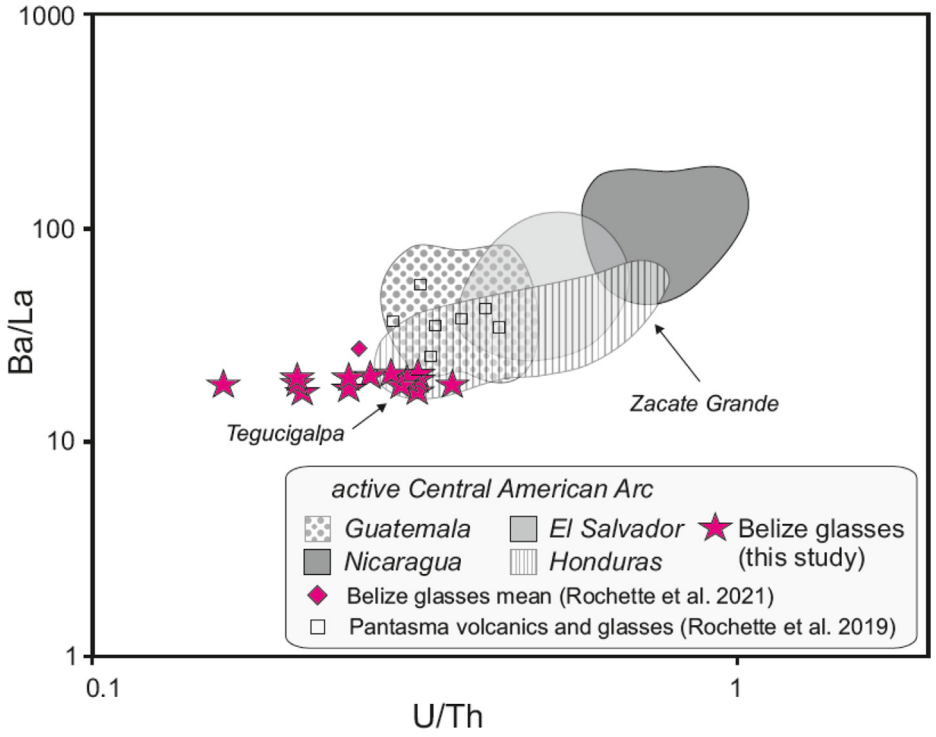

Fig. 7. Plot of Ba/La vs. U/Th ratios for Belize glasses in comparison to values from the Central American arc (data from Alves et al., 2002), whose scatter represents along-arc slab-mantle interactions; comparison data for Belize glasses and Pantasma volcanics and glasses from Rochette et al. (2019, 2021).

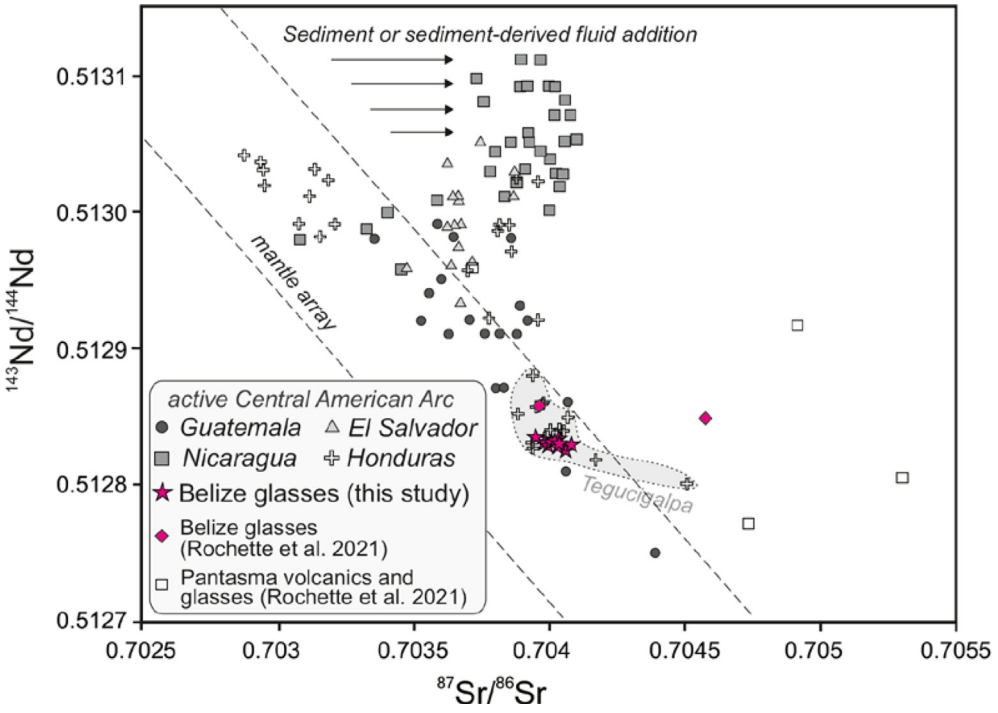

Fig. 8. Plot of $^{143}Nd/^{144}Nd$ ratios versus $^{87}Sr/^{86}Sr$ ratios of Belize glasses together with reference fields for active Central American arc samples (Carr et al., 1990, 2003; Patino et al., 1997, 2000; Walker et al., 2000, 2001); comparison data for Belize glasses and Pantasma volcanics and glasses from Rochette et al. (2021).

Table 5
Concentrations and interelement ratios of highly siderophile elements (Re, Os, Ir and Pt) and Re-Os isotope data (including replicate analyses of unspiked samples) for selected Belize tektites.

Sample	Re ppb	Os ppb	Ir ppb	Pt ppb	$^{187}Os/^{188}Os$	$^{187}Re/^{188}Os$	Os/Ir	Pt/Ir
B02	0.191	0.001	0.043	26.943	0.2487 (22)	920.07	0.023	626.6
B02	–	–	–	–	0.282 (48)	–	–	–
B04	0.396	0.002	0.086	16.099	0.3316 (36)	969.31	0.023	187.2
B05	0.169	0.002	0.145	1.197	0.1350 (70)	414.20	0.014	8.26
B05	–	–	–	–	0.156 (14)	–	–	–
B06	1.946	0.001	0.035	2.246	0.337 (90)	9354.5	0.029	64.17
B06	–	–	–	–	0.349 (40)	–	–	–
B07	–	0.005	–	–	1.322 (72)	–	–	–
B07	–	–	–	–	1.265 (90)	–	–	–

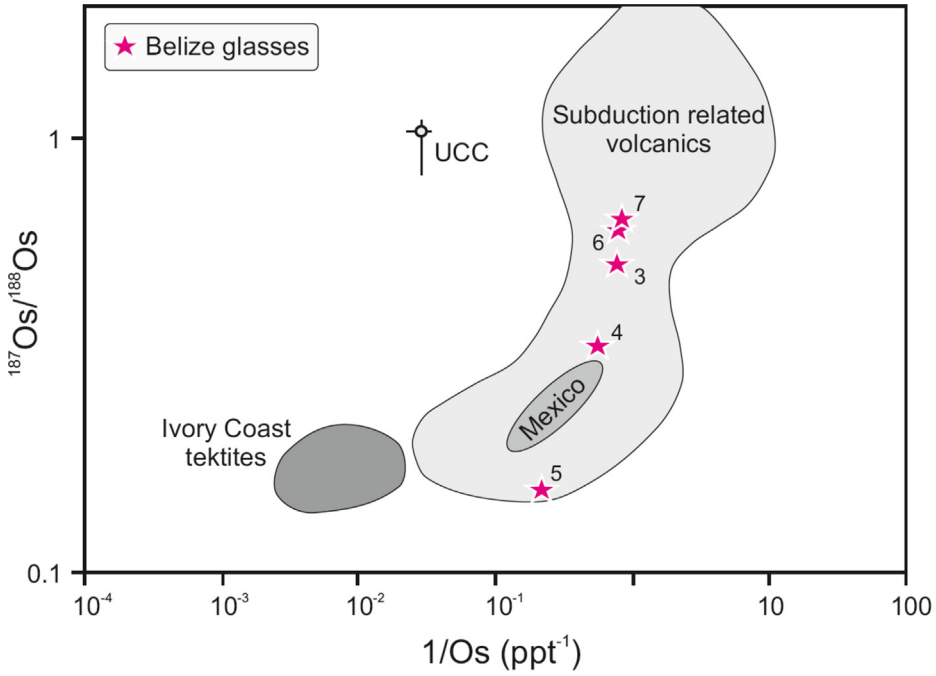

Fig. 9. Present-day $^{187}Os/^{188}Os$ ratios versus the inverse of Os concentrations in Belize glasses in comparison to arc lavas from world-wide locations (Alves et al., 2002), Ivory Coast tektites (Koeberl and Shirey, 1993) and the average Upper Continental Crust (Peucker-Ehrenbrink and Jahn, 2001).

[Rochette et al., 2021] and 1.07 Ma for Ivory Coast tektites [Koeberl et al., 1997]) increases the spread, although it does not erase the overlap of their uncertainties. The similarity of ^{10}Be contents likely reflects a fortuitous combination of precipitation rates, source grain properties, and grain histories.

4. DISCUSSION

4.1. Petrography

The size and shapes of the Belize glasses are similar to those of other Cenozoic tektites. Like other Cenozoic tektites, the Belize glasses contain vesicles, lechatelierite, and schlieren but no crystallites/microlites. The dark inclusions observed in lechatelierite particles in specimens B4, B9, B15, and B18 have not previously been observed in other tektites. As discussed above, two inclusions in B18, with dark opaque or brown regions, do not appear to be lechatelierite particles. At least one lechatelierite particle has a ballen-like texture. With these exceptions, most (14) of the specimens are petrographically indistinguishable from other Cenozoic tektites.

4.2. Geochemistry

The trace element patterns of the Belize glasses plotted in Fig. 5 follow closely the trace element patterns of rocks from the Central American Arc. Trace element ratios and isotopic signatures aid in the search for a source region. In general, however, the trace element abundances do not form/occur in patterns that can be used to confirm an impact origin (although this is similar to other tektites).

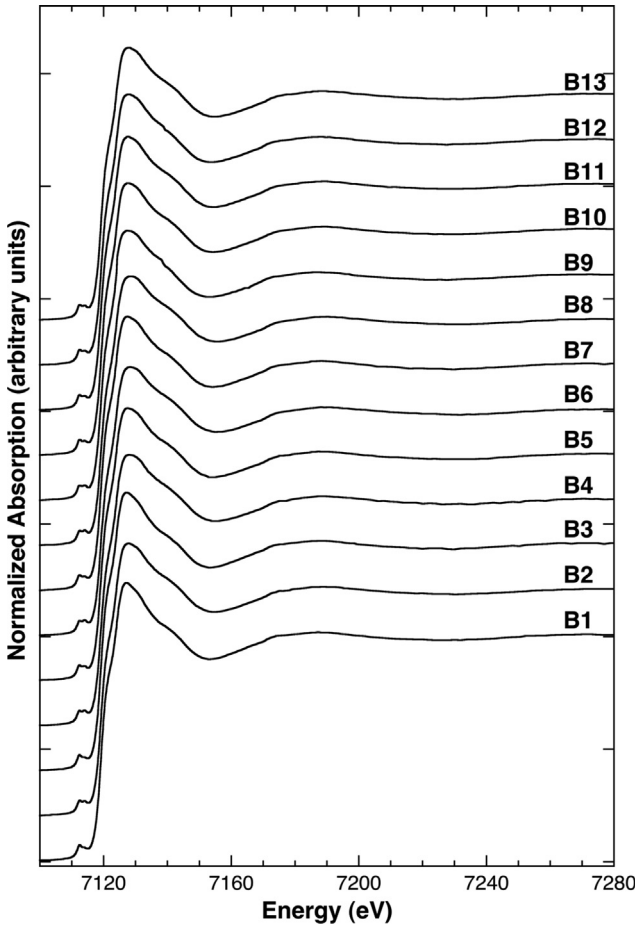

Fig. 10. Experimental Fe K-edge XANES spectra of the Belize glasses. The spectra are normalized to unit intensity at the high energy side. General shape and energy position of the XAS features are consistent with those reported for XANES spectra of tektites.

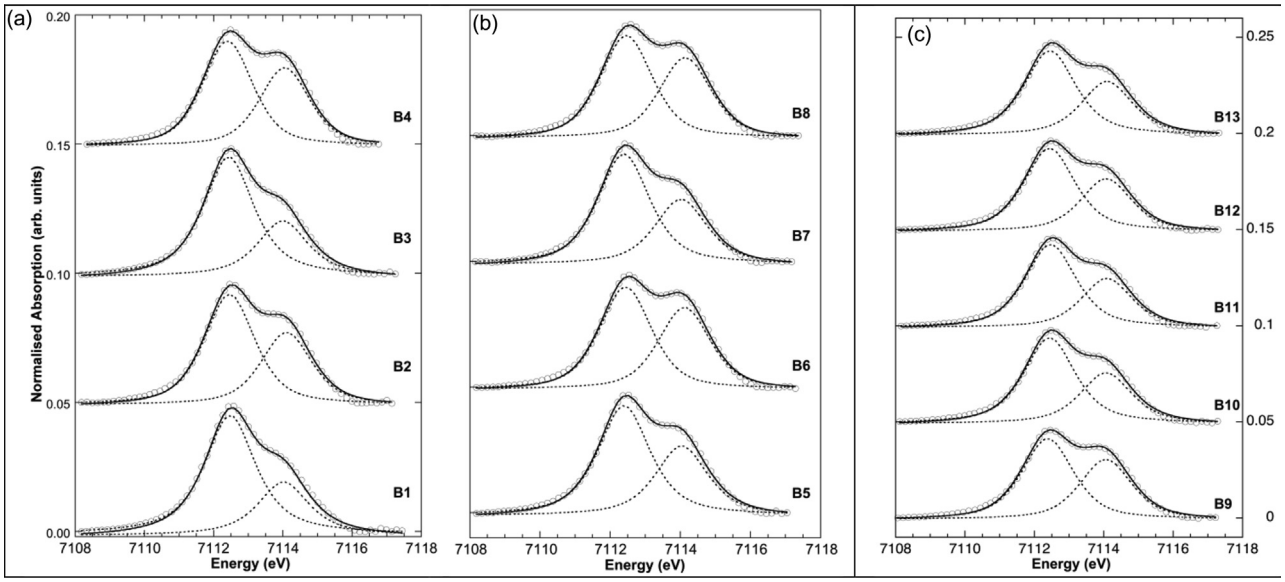

Fig. 11. Background subtracted pre-edge peaks of the studied glasses (empty circles) along with the pseudo-Voigt component used in the fitting procedures (dotted lines), and pseudo-Voigt sums (solid lines). Each pre-edge peak could be fitted with two components (see text).

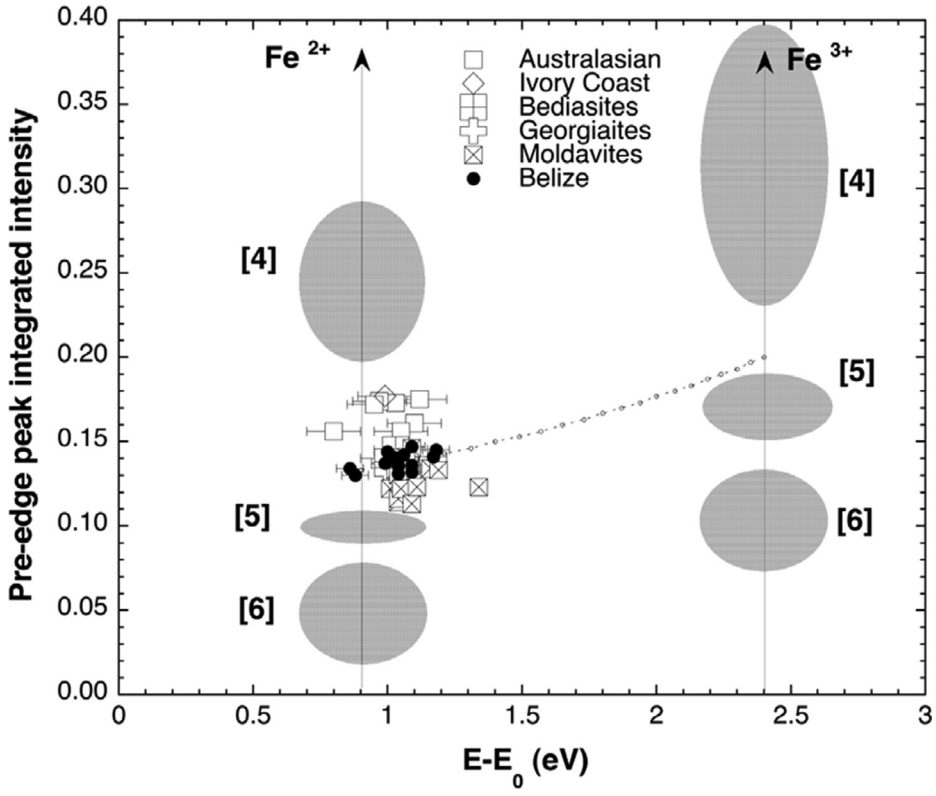

Fig. 12. Plot of the pre-edge peak integrated intensity vs. centroid energy position. Solid symbols refer to the Belize glasses studied here, whereas empty circles refer to tektites from the known four strewn fields already studied in the literature. The dotted line with small circles is a mixing line calculated in order to evaluate the ratio between Fe^{2+} and Fe^{3+} species. (Data for other tektites: Wilke et al., 2001; Farges, 2001; Giuli et al., 2002, 2008).

Table 6
XANES (iron oxidation data), density, and water content for Belize glass samples.

Sample	$Fe^{2+}/(Fe^{2+}+Fe^{3+})$	Density*	Water (ppm)
B1	<0.01	2.538	119
B2	0.09	2.539	111
B3	<0.01	2.537	120
B4	0.09	2.471	121
B5	0.05	2.539	133
B6	0.13	2.539	96
B7	0.04	2.532	118
B8	0.14	2.555	123
B9	0.10	2.548	133
B10	0.06	2.495	104
B11	0.07	2.542	99
B12	0.07	2.540	101
B13	0.08	2.538	82

*Calculated (see text).

Lavas from the Central American Arc define local and regional geochemical trends that reflect variations in slab-mantle interactions (Patino et al., 2000). Varying contributions of sedimentary units involved in the subduction process of the Cocos plate underneath the Caribbean plate along the Central American Arc and the corresponding changes in the geochemistry of several key elements potentially provide a proxy for the derivation and source region of the glasses from Belize. For example, Ba/La and U/Th ratios (Patino et al., 2000) are distinctive indicators of the source region. Compositional variations of these indicators in the rocks are shown in Fig. 7 and are compared to the Belize glasses analyzed in this study.

The Belize samples are distinct from the volcanics of the Nicaragua and El Salvador region, whereas arc lavas from Guatemala and, especially, Honduras plot in close proximity to the Belize glasses. The Belize glasses also partially overlap the field for the Tegucigalpa volcano in Honduras. As the geographical extent of this volcanic area is small, the match may be coincidental and should not be overinterpreted. The Pantasma structure in the north of Nicaragua was proposed as a possible source crater of the Belize glasses (Povenmire and Cornec, 2015; Povenmire, 2016; and Rochette et al., 2021), based partly on good agreement of $^{40}Ar/^{39}Ar$ ages of about 800 Ma. As with isotope data in Fig. 4, average Belize glass data from Rochette et al. (2021) fit well with our data, whereas Pantasma crater data (Rochette et al., 2019) are more widely scattered (Fig. 7). Also, as there are some significant differences to Nicaraguan arc samples with respect to some geochemical composition, further investigations regarding a possible source in that region will be necessary.

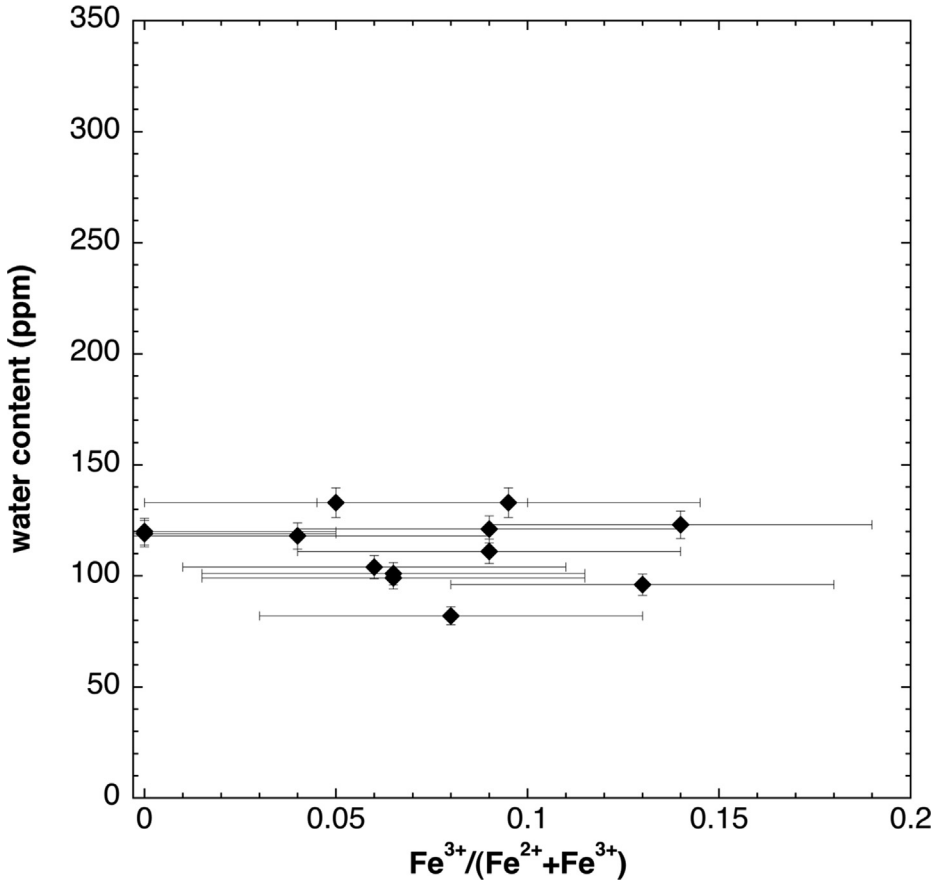

Fig. 13. Water content of the studied Belize glasses vs. XAS-derived $Fe^{3+}/(Fe^{2+}+Fe^{3+})$ ratio. Both the water content (ranging from 80 to 132 ppm) and the $Fe^{3+}/(Fe^{2+}+Fe^{3+})$ ratio are consistent with literature data on tektites.

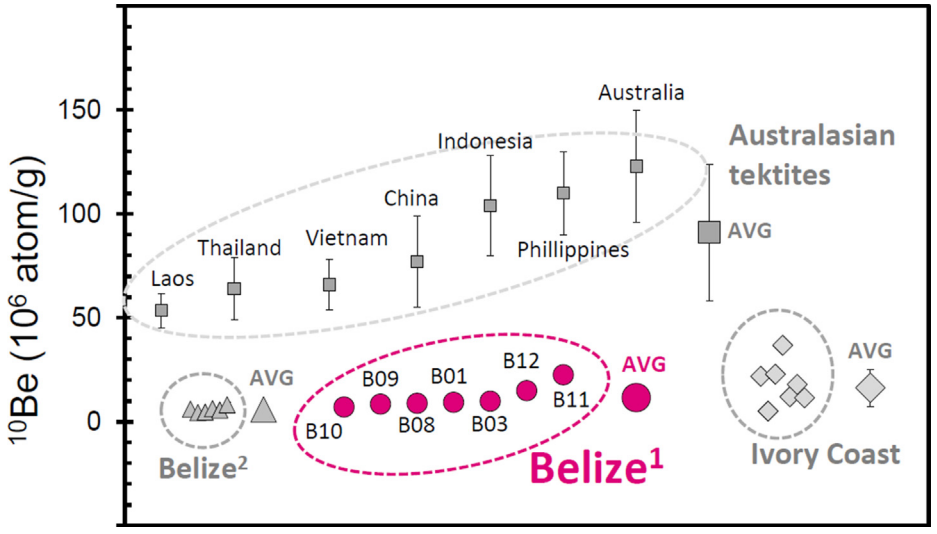

Fig. 14. ^{10}Be concentrations of Belize tektites and other tektites. All concentrations are re-normalized to a ^{10}Be half-life of 1.36 Ma (Nishiizumi et al., 2007). Belize[1] (this work), Belize[2] (Rochette et al., 2021), Australasian tektites (Ma et al., 2004), Ivory Coast (Serefiddin et al., 2007). The x-axis has no general significance, except that for Australasian tektites the data are plotted with increasing distance from the central Indochina region.

Table 7
^{10}Be concentrations [10^6 atom/g][1] of Belize glasses and tektites from classical strewn fields.

Belize glasses[2]		Ivory Coast tektites[3]		Australasian tektites[4]	
B01	9.4 ± 1.4	IVC2096	21.9 ± 0.5	Laos	53.5 ± 8.2
B03	9.9 ± 1.7	IVC3395	5.1 ± 0.3	Thailand	64 ± 15
B08	8.89 ± 2.6	IVC3396	22.9 ± 1.2	Vietnam	66 ± 12
B09	8.5 ± 1.7	IVC8901	36.8 ± 0.7	China	77 ± 22
B10	7.1 ± 1.5	IVC8902	12.1 ± 0.3	Indonesia	104 ± 24
B11	22.6 ± 1.8	IV0622304	18.0 ± 0.8	Philippines	110 ± 20
B12	15.0 ± 1.9	IV07022304B	11.5 ± 0.6	Australia	123 ± 27
Average[5]	11.6 ± 5.4	Average	16.3 ± 9.0	Average	91 ± 33

Notes: (1) All concentrations referenced or re-normalized to a ^{10}Be half life of 1.36 Ma (Nishiizumi et al., 2007); see text. (2) This work. (3) Serefiddin et al. (2007). (4) Ma et al. (2004). (5) ± 1σ.

4.3. Isotope geochemistry

The Nd and Sr isotopic data resolve the existence of different mantle reservoirs beneath Central America and the input of different mixing end-members, such as granitic or metamorphic basement and carbonate sediment that contribute to the formation of the magmatic products (e.g., Feigenson et al. 2004). The isotopic data, like the trace element ratios mentioned above, can be used to identify the origin of magmatic material along the arc. There is a systematic variation of mantle components and their admixtures. The identities of these components can be seen in the ^{143}Nd/^{144}Nd versus ^{87}Sr/^{86}Sr diagram (Fig. 8). The data define two trends, one with a negative slope following the mantle array, which is defined by mid ocean ridge basalts and ocean island basalt representing melts from the upper and lower mantle, and a second trend with a positive slope. The most affected samples of the second trend are those of the magmatic products from the volcanic front of Nicaragua. Samples are characterized by Nd isotopes similar to MORB, but more radiogenic ^{87}Sr/^{86}Sr ratios, resulting from sediment or sediment-driven fluid addition (Feigenson et al. 2004). This defines a specific array for the Nicaragua samples which is clearly segregated from the Belize glasses which are in good agreement with magmatic products from Honduras and Guatemala. Comparison with Belize and Pantasma data (Rochette et al., 2021) yield similar scatter as noted above for the data in Figs. 4 and 7.

The Belize glasses occupy a unique position in the ^{143}Nd/^{144}Nd versus ^{87}Sr/^{86}Sr diagram (Fig. 8). Specifically, they plot on the mantle array in the region of positive εNd and slightly negative εSr. The irghizites and low-silica zhamanshinites from the Zhamanshin impact structure (Kazakhstan) plot close to the Belize glasses, but εSr for these samples is slightly positive, rather than negative. All other tektites and impact glasses plot in the continental crust array, well away from the Belize glasses. Any correlation with the Australasian tektites, which are of the same age, is ruled out by this observation.

The Os isotopic compositions of world-wide arc lavas were shown to span a very large range of ^{187}Os/^{188}Os values, from abyssal peridotite-like to more radiogenic, crust-like values (e.g., Alves et al. 2002). Such arc lavas also exhibit extremely low Os contents (mostly < 10 ppt) compared to both upper continental crust (~31 ppt; Peucker-Ehrenbrink and Jahn, 2001), and mantle peridotites (up to <5 ppb; e.g., Meisel et al. 2001). Alves et al. (2002) claimed that such low Os contents may reflect the compatible behavior of Os during mantle melting and (to a lesser extent) fractional crystallization. The range for subduction-related volcanics from worldwide locations with respect to Re-Os isotopes and Os elemental abundances is shown in Fig. 9. The glasses from Belize overlap with this range and, thus, could demonstrate their close relationship with subduction-related volcanics. The only arc lavas in proximity to the Belize strewn field that were analyzed for osmium systematics are from Mexico and, although not directly related to the Central American Arc, are also shown in Fig. 9.

However, the Belize samples analyzed in this study exhibit Ir concentrations ranging from UCC-like (~22 ppt; Peucker-Ehrenbrink and Jahn, 2001) to significantly supercrustal values (e.g., 145 ppt Ir in sample B05). These Ir concentrations roughly correlate with the ^{187}Os/^{188}Os ratios. Sample B05 exhibits the highest Ir content and a near to chondritic ^{187}Os/^{188}Os of ~0.135, whereas sample B06, with an Ir content of 35 ppt exhibits a significantly more radiogenic ^{187}Os/^{188}Os ratio of ~0.337. Interestingly, such signatures (strong Os depletion in conjunction with elevated Ir contents and near chondritic ^{187}Os/^{188}Os ratios) have been observed in impact glasses from various localities/locations world-wide (e.g., Ackerman et al., 2017, 2019; Jonášová et al., 2016) and where interpreted to reflect Os loss in the superheated tektite melt and the addition of a meteoritic component. Irghizites from the Zhamanshin impact structure, for example, while exhibiting consistently low ^{187}Os/^{188}Os ratios of around ~0.13 and subcrustal Os concentrations of mostly 1 to 5 ppt, have Ir concentrations of up to 160 ppt (Jonášová et al., 2016). Similar signatures were also observed in moldavites and Australasian tektites (Ackerman et al., 2017, 2019). Although comparable to Os signatures of different types of arc lavas from around the world, our data for Belize glasses can, therefore, also interpreted in line with additions of meteoritic components to some of the Belize glasses, followed by Os-loss in the impact vapor plume. This could explain their very low Os/Ir ratios of around ~0.2 and exceptionally high ^{187}Re/^{188}Os ratios of

~869 to ~9354. Notably, Belize sample B05, with a chondrite-like $^{187}Os/^{188}Os$ ratio, also exhibits a Pt/Ir ratio of ~8.3 (in comparison to values of up to ~627 in the other analyzed samples). This ratio lies between the UCC and the chondritic value (~23.2 Pt/Ir in the UCC vs. 2.03 Pt/Ir in CI chondrites; Peucker-Ehrenbrink and Jahn, 2001; Tagle and Berlin 2008).

Instead of simply reflecting HSE concentrations and $^{187}Re/^{188}Os$ and $^{187}Os/^{188}Os$ isotope signatures of their (probably arc-like) parent material (Fig. 8), the huge range in $^{187}Os/^{188}Os$ ratios in the samples analyzed in this study (ranging from near-chondritic to supercrustal values) in conjunction with their consistently low Os- and up to supercrustal Ir concentrations can, therefore, also be interpreted as a minor and heterogeneous meteoritic component in the Belize glass. This is supported by the recently published Cr-isotopic data that indicate a (minor) chondritic component in some other Belize glass samples (Rochette et al., 2021).

4.4. Fe oxidation state and water content

The $Fe^{3+}/(Fe^{3+} + Fe^{2+})$ ratios of 13 samples analyzed by Fe K-edge XANES have been determined to vary between 0.0 and 0.14 ± 0.05, consistently with values for tektites from the four "classical" strewn fields. Also the general shape of XANES spectra, which is dependent on the Fe coordination geometry, is perfectly consistent with data presented in the literature for tektite glasses.

Water content, as determined by micro-FTIR, varies from 82 to 133 ppm, consistent with available data on tektites and microtektites (Koeberl and Beran, 1988; Beran and Koeberl, 1997, Giuli et al., 2013). On the whole, both the low $Fe^{3+}/(Fe^{3+} + Fe^{2+})$ ratios and the low water content are compatible with available data on tektites.

4.5. Be-10 measurements

In situ production does not appear to be a major contributor to the ^{10}Be inventory in Belize glasses. At the latitude, 17°N, and mean elevation, 173 m, of Belize, the production rate at the very surface is ~2 atom $^{10}Be\ g^{-1}\ a^{-1}$. After a few million years, a theoretical *maximum* ^{10}Be concentration of $\sim 4 \times 10^6$ atom/g could be produced. An exposure at the surface for this long is improbable since it would require that: (1) the period of irradiation began well before the time of the glass-forming event and continued uninterruptedly to the present; and (2) the source material remained close to the surface throughout and somehow escaped erosion, unlikely in this setting. We believe that the $^{40}Ar/^{39}Ar$ age (~0.8 Ma) of the Belize glasses sets a considerably shorter and more realistic upper bound on the duration of irradiation and hence on the amount of *in situ* production. After 0.8 Ma of irradiation, we would expect to have a ^{10}Be concentration of $\sim 1 \times 10^6$ atom/g, or, at most, about 1/6 of the observed values. Measurements of ^{36}Cl could help refine this conclusion.

An extraterrestrial source for the ^{10}Be in Belize glasses is excluded based on other geochemical measurements; in general tektites contain very low amounts of meteoritic material, as is the case here, too. Like the ^{10}Be in the Australasian tektites, the ^{10}Be found in the Belize glasses is dominated by meteoric input. A complete analogy between the two sets of glasses would have both formed from impacts into loosely consolidated target material. By themselves, however, the ^{10}Be concentrations of the Belize glasses do *not* require such material at the time of an impact. Volcanic rocks collected in Middle America contain from 0.6×10^6 to 14.5×10^6 atom $^{10}Be/g$, from subducted oceanic sediment (Morris and Tera, 1989; their Table 3). Morris and Tera argued against *in situ* production of ^{10}Be on the basis of constant $^{10}Be/^{9}Be$ ratios in mineral separates and against assimilation of soils—although with less certainty—on the basis of low ^{10}Be determinations in geographic regions where assimilation might have been expected. The key point is that the Belize glasses have ^{10}Be contents in the same range as, and hence *could* have been derived directly from, subducted lava, and may subsequently have been isolated from local rain water, ground water, and cosmic rays.

Even so, we are not inclined to set much stock in this possibility. First, the so-far limited ranges of ^{10}Be concentrations Belize glasses – a factor of two or three perhaps – implies sampling of a relatively uniform source and it is not clear whether Belize volcanics fit this description. Second, and perhaps more persuasively, given a) the many similarities between the Belize glasses and the main-group tektites, and b) the near certainty that none of the latter has a rocky precursor, a rocky precursor for the Belize glasses seems unlikely.

5. SUMMARY AND CONCLUSIONS

Over the past two decades, reports on tektite-like glasses from an area in Belize have been published. Earlier data indicated an age that is identical, within error, to that of Australasian tektites, but with some compositional differences, leading to suggestions of either a new tektite strewn field or an association with the Australasian strewn field. In this study we used a variety of petrographic and geochemical methods to thoroughly study and analyze a set of (up to) 18 Belize glasses. The aims were to determine their compositional variation, their mode of formation and possible source rocks, and their relation to known tektites, and to search for evidence of an extraterrestrial component.

Petrographically, the Belize glasses show close similarities to tektites from the four "classical" strewn fields, with the presence of lechatelierites, schlieren, and vesicles, which are widely accepted indicators of an impact origin. No comparable similarities to volcanic glasses are evident (see also criteria in Ferrière et al., 2021). The geochemical and isotopic data presented here also allow for, but do not provide unambiguous evidence of, an impact origin. This second generalization is consistent with observations for "normal" Cenozoic tektites, most of which have compositions almost identical to that of upper terrestrial continental crust, with at best, a rare and minor admixture of a meteoritic component. Even though the extent of the strewn field is not yet clearly established, we conclude that the similarities to tektites justify that the Belize glasses are called "tektites". We make the following observations and conclusions:

(i) An impact origin of the Belize glasses is indicated by several lines of evidence, principally the absence of primary crystallites/microlites, the presence of lechatelierite, and their low water content;
(ii) Cr, Co and Ni elemental abundances and interelement ratios, as well as trace element patterns are typical for local and regional volcanics from the active Central American arc;
(iii) Trace element patterns confirm a close correlation with volcanics from the Central American arc, and, in particular, are consistent with an the Belize glasses being derived from material similar to volcanic rocks from Honduras or Guatemala;
(iv) These observations are confirmed by Sr-Nd isotope signatures of the Belize glasses, showing close similarities to Central American volcanics in general, and Honduran and Guatemalan volcanic, in particular. Our data do not necessarily indicate derivation of the glasses from Nicaragua, as advocated by Povenmire et al. (2011) or Rochette et al. (2021);
(v) Osmium concentrations and $^{187}Os/^{188}Os$ ratios are comparable to arc volcanics from world-wide locations. However, elevated Ir concentrations of up to 145 ppt, in conjunction with near-chondritic Pt/Ir and $^{187}Os/^{188}Os$ ratios (sample B05), can also be interpreted with the admixture of a slight meteoritic component to some of the Belize samples. This agrees with Cr-isotope data recently published by Rochette et al. (2021). In that case, the consistently low Os abundances (of 1 to 5 ppt) might result from Os-loss in an overheated "tektite"-melt or inside an impact vapor plume, comparable to conclusions drawn for Central European and Australasian tektites as well as irghizites from the Zhamanshin impact structure (Jonášová et al., 2016; Ackerman et al., 2017, 2019; Schulz et al., 2020).
(vi) ^{10}Be concentrations are not determinative of origin. They are consistent with values typical of both, young or deeply buried soils and with values for Central American volcanics, which carry subducted ^{10}Be.
(vii) The iron oxidation state values determined by XANES and the low water contents as determined by micro-FTIR are consistent with values for tektites from the four "classical" strewn fields.

Geochemical data so far clearly indicate a source different from that of the Australasian tektites. Both isotope data sets for the Belize glasses indicate a close relationship to local arc lavas, especially those from Guatemala and Honduras, supporting the claim that the glasses were not transported far from their source (e.g., volcano or impact crater). Our data are agnostic regarding any particular source crater, in contrast to what was suggested/concluded by Rochette et al. (2021). The primary evidence for the impact origin of these glasses rests, therefore, on the petrographic characteristics and the low water content, and the $Fe^{3+}/(Fe^{3+}+Fe^{2+})$ ratios as presented in this work. The evidence from ^{10}Be is consistent with, but does not require, a model of formation for the Belize glasses by an impact on loosely consolidated surface sediments exposed to rain.

Declaration of Competing Interest

The authors declare that they have no known competing financial interests or personal relationships that could have appeared to influence the work reported in this paper.

ACKNOWLEDGEMENTS

This paper is dedicated to the memory of S. Ross Taylor (1925-2021); even though he is best known for his lunar research, he was probably the first, over 60 years ago, to use detailed geochemical analyses to provide evidence for a terrestrial impact origin of tektites when most researchers (in absence of actual analyses of lunar rocks) still believed that they were lunar volcanic glasses.

We are grateful to J. Cornec (Denver, USA) for providing the Belize glass samples (and sample location/geology information) for this study, to D. Topa (Natural History Museum Vienna) for help with the SEM and microprobe work, and to D. Mader (University of Vienna) for help with the trace element analyses. This is contribution 71 of the DFG-funded ICP-MS facilities at the Steinmann-Institute, University of Bonn. We are grateful to David T. King Jr. and an anonymous reviewer, as well as AE Yuri Amelin, for very helpful reviews and comments.

APPENDIX A. SUPPLEMENTARY MATERIAL

Supplementary data to this article can be found online at https://doi.org/10.1016/j.gca.2022.02.021.

REFERENCES

Ackerman L., Magna T., Žák K., Skála R., Jonášová Š., Mizera J. and Řanda Z. (2017) The behavior of osmium and other siderophile elements during impacts: insights from the Ries impact structure and central European tektites. *Geochim. Cosmochim. Acta* **210**, 59–70.

Ackerman L., Skála R., Křížová Š., Žák K. and Magna T. (2019) The quest for an extraterrestrial component in Muong Nong-type and splash-form Australasian tektites from Laos using highly siderophile elements and Re-Os isotope systematics. *Geochim. Cosmochim. Acta* **252**, 179–189.

Alves S., Schiano P., Capmas F. and Allegre C. J. (2002) Osmium isotope binary mixing arrays in arc volcanism. *Earth Planet. Sci. Lett.* **198**, 355–369.

Barrat J. A., Jahn B. M., Amosse J., Rocchia R., Keller F., Poupeau G. R. and Diemer E. (1997) (1997) Geochemistry and origin of Libyan Desert glasses. *Geochim. Cosmochim. Acta* **61**, 1953–1959.

Beran A. and Koeberl C. (1997) Water in tektites and impact glasses by Fourier-Transformed Infrared Spectrometry. *Meteoritics Planet. Sci.* **32**, 211–216.

Birck J. L., Roy B. M. and Capmas F. (1997) Re-Os isotopic measurements at the femtomole level in natural samples. *Geostandards Newslett.* **20**, 19–27.

Blum J. D., Papanastassiou D. A., Koeberl C. and Wasserburg G. J. (1992) Nd and Sr isotopic study of Australasian tektites: New constraints on the provenance and age of target materials. *Geochim. Cosmochim. Acta* **56**, 483–492.

Brown G. E., Farges F., and Calas G. (1995) X-ray scattering and X-ray spectroscopy studies of silicate melts. In *Structure, Dynamics and Properties of Silicate Melts* (eds. J. F. Stebbins, P. F. McMillan, D. B. Dingwell), *Review in Mineralogy*, **vol. 32**, pp. 317–410.

Calas G. and Petiau J. (1983) Coordination of iron in oxide glasses through high-resolution K-edge spectra: information from the pre-edge. *Solid State Commun.* **48**, 625–629.

Carr M. J. and Pontier N. K. (1981) Evolution of a young parasitic cone towards a mature central vent; Izalco and Santa Ana volcanoes in El Salvador, Central America. *J. Volcanol. Geoth. Res.* **11**, 277–292.

Carr M. J. and Walker J. A. (1987) Intra-eruption changes in composition of some mafic to intermediate tephras in Central America. *J. Volcanol. Geoth. Res.* **33**, 147–159.

Carr M. J., Feigenson M. D. and Bennett E. A. (1990) Incompatible element and isotopic evidence for tectonic control of source mixing and melt extraction along the Central American arc. *Contrib. Miner. Petrol.* **105**, 369–380.

Carr M., Feigenson M., Patino L., and Walker J. (2003) Volcanism and geochemistry in Central America: Progress and problems. In: *Inside the Subduction Factory. American Geophysical Union* (Ed. Eiler J.M.). *Geophysical Monograph Series*, **vol. 133**, pp. 153–174.

Chapman D. R., Larson H. K. and Schreiber L. (1984) Population polygons of tektite specific gravity for various localities in Australasia. *Geochim. Cosmochim. Acta* **28**, 821–839.

Chmeleff J., von Blanckenburg F., Kossert K. and Jakob D. (2010) Determination of the ^{10}Be half-life by multicollector ICP-MS and liquid scintillation counting. *Nuclear Instrum. Meth. Phys. Res. B* **263**, 192–199.

Cohen A. S. and Waters F. G. (1996) Separation of osmium from geological materials by solvent extraction for analysis by thermal ionisation mass spectrometry. *Anal. Chim. Acta* **332**, 269–275.

Cornec J., Cornec L., and Povenmire H. (2013) A layered tektite from the Central American strewn field. In *44th Lunar and Planetary Science Conference*, abstract no. 1123.

Dunlap R. A. and Sibley A. D. E. (2004) A Mössbauer effect study of Fe site occupancies in Australasian tektites. *J. Non-Cryst. Solids* **337**, 36–41.

Dunlap R. A., Eelman D. A. and MacKay G. R. (1998) A Mössbauer effect investigation of correlated hyperfine parameters in natural glasses (tektites). *J. Non-Cryst. Solids* **223**, 141–146.

Farges F. (2001) Crystal-chemistry of Fe in natural grandidierites: a XAFS spectroscopy study at the Fe K-edge. *Phys. Chem. Minerals* **28**, 619–629.

Feigenson M. D., Carr M. J., Maharaj S. V., Juliano S. and Bolge L. L. (2004) Lead isotope composition of Central American volcanoes: Influence of the Galápagos plume. *Geochem. Geophys. Geosyst.* **5**, Q06001. doi.10.1029/2003GC000621.

Ferrière L., Crósta A. P., Wegner W., Libowitzky E., Iwashita F. and Koeberl C. (2021) Distinguishing volcanic from impact glasses – The case of the Cali glass (Colombia). *Geology* **49**, 1421–1425.

Fudali R. F., Dyar M. D., Griscom D. L. and Schreiber D. (1987) The oxidation state of iron in tektite glass. *Geochim. Cosmochim. Acta* **51**, 2749–2756.

Gilchrist J., Thorpe A. N. and Senftle F. E. (1969) Infrared analysis of water in tektites and other glasses. *J. Geophys. Res.* **74**, 1475–1483.

Giordano D., Russell J. K. and Dingwell D. B. (2008) Viscosity of magmatic liquids: A model. *Earth Planet. Sci. Lett.* **271**, 123–134.

Giuli G., Pratesi G., Paris E. and Cipriani C. (2002) Fe local structure in tektites by EXAFS and high resolution XANES spectroscopy. *Geochim. Cosmochim. Acta* **66**, 4347–4353.

Giuli G., Eeckhout S. G., Koeberl C., Pratesi G. and Paris E. (2008) Yellow impact glass from the K/T boundary at Beloc (Haiti): XANES determination of the Fe oxidation state and implications for formation conditions. *Meteoritics Planet. Sci.* **43**, 981–986.

Giuli G., Eeckhout S.G., Cicconi M.R., Koeberl C., Pratesi G., and Paris E. (2010a) Iron oxidation state and local structure in North American tektites. In *Large Meteorite Impacts and Planetary Evolution IV* (eds. W. U. Reimold and R. Gibson), *Geological Society of America Special Paper*, **vol. 465**, pp. 645–652.

Giuli G., Pratesi G., Eeckhout S.G., Koeberl C., and Paris E. (2010b) Iron reduction in silicate glass produced during the 1945 nuclear test at the trinity site (Alamogordo, New Mexico, USA). In *Large Meteorite Impacts and Planetary Evolution IV* (eds. W. U. Reimold and R. Gibson), *Geological Society of America Special Paper*, **vol. 465**, pp. 653–662.

Giuli G., Paris E., Hess K. U., Dingwell D. B., Cicconi M. R., Eckhout S. G., Fehr K. T. and Valenti P. (2011) XAS determination of the Fe local environment and oxidation state in phonolite glasses and implications for the viscosity of silicate melts. *American Mineral.* **96**, 631–636.

Giuli G., Cicconi M. R. and Paris E. (2012) $^{[4]}Fe^{3}$+-O distance in synthetic kimzeyite garnet, $Ca_3Zr_2[Fe_2SiO_{12}]$. *European Journal of Mineralogy* **24**, 783–790.

Giuli G., Cicconi M. R., Eeckhout S. G., Koeberl C., Glass B. P., Pratesi G., Cestelli-Guidi M. and Paris E. (2013) North-American microtektites are more oxidized than tektites. *American Mineral.* **98**, 1930–1937.

Glass B. P. (1984) Solution of naturally-occurring glasses in the geological environment. *J. Non-Cryst. Solids* **67**, 265–286.

Govindaraju K. (1989) compilation of working values and sample description for 272 geostandards. *Geostandard. Newslett.* **13**, 1–113.

Hildebrand A. R., Moholy-Nagy H., Koeberl C., Senftle F., Thorpe A. N., Smith P. E. and York D. (1994) Tektites found in the ruins of the Maya city of Tikal, Guatemala (Abstract). *Lunar and Planetary Science* **XXV**, 549–550.

Izett G. and Meeker G. (1995) ^{40}Ar/^{39}Ar age and composition of tektites from Belize. *Geol. Soc. Am. Abstr. Programs* **6**, A-207.

Jarosewich E., Clarke R. S. J. and Barrows J. N. (1987) The Allende meteorite reference sample. *Smithson. Contrib. Earth Sci.* **27**, 1–49.

Jonášová Š., Ackerman L., Zak K., Skála R., Ďurišová J., Deutsch A. and Magna T. (2016) Geochemistry of impact glasses and target rocks from the Zhamanshin impact structure. *Geochim. Cosmochim. Acta* **190**, 239–264.

Jourdan F., Nomade S., Wingate M. T. D., Eroglu E. and Deino A. (2019) Ultraprecise age and formation temperature of the Australasian tektites constrained by ^{40}Ar/^{39}Ar analyses. *Meteoritics Planet. Sci.* **54**, 2573–2591.

King E. A. (1964) *Investigations of North American tektites* Dissertation. Department of Geology, Harvard University, Harvard, Cambridge, MA.

King Jr., D. T., Cornec J. H., Petruny L. W., and Zou H. (2016a) Tektites of Western Belize – Characteristics and possible origin. In *47th Lunar and Planetary Science Conference*, abstract no. 2910.

King, Jr., D. T., Petruny L. W., Cornec J. H., Rochette P. and Milham D. (2016) Petrographic characteristics of some tektites from Western Belize. *Geol. Soc. Am. Abst. Prog.* **48**(7). Abstract 2016AM-284396.

King, Jr., D. T., Cornec J., Petruny L. W., Milham D., Holland B., Ricketts S., Myers N. R., Weber R. D. and George R. (2018) Sedimentary characteristics and geological history of the Cenozoic Red Bank group, northern Belize. *Gulf Coast Assoc. Geol. Soc. Trans.* **68**, 269–284.

Koeberl C. (1993) Instrumental neutron-activation analysis of geochemical and cosmochemical samples – A fast and reliable method for small sample analysis. *J. Radioanalyt. Nuclear Chem.* **168**, 47–60.

Koeberl C. (1994) Tektite origin by hypervelocity asteroidal or cometary impact: Target rocks, source craters, and mechanisms. In *Large Meteorite Impacts and Planetary Evolution* (eds. B. O. Dressler, R. A. F. Grieve and V. L. Sharpton), Boulder: *Geological Society of America Special Paper*, **vol. 293**, pp. 133–151.

Koeberl C. (2014) The geochemistry and cosmochemistry of impacts. In *Treatise on Geochemistry*, second ed., **vol. 2** (eds. H. D. Holland and K. K. Turekian) (Planets, Asteroids, Comets and The Solar System). Oxford: Elsevier, pp. 73–118.

Koeberl C. and Beran A. (1988) Water content of tektites and impact glasses and related chemical studies. In *Proceedings, 18th Lunar and Planetary Science Conference*. LPI-Cambridge University Press, pp. 403–408.

Koeberl C. and Shirey S. B. (1993) Detection of a meteoritic component in Ivory Coast tektites with rhenium-osmium isotopes. *Science* **261**, 595–598.

Koeberl C., Bottomley R., Glass B. P. and Storzer D. (1997) Geochemistry and age of Ivory Coast tektites and microtektites. *Geochimica et Cosmochimica Acta* **61**, 1745–1772.

Korschinek G., Bergmaier A., Faestermann T., Gerstmann U. C., Knie K., Rugel G., Wallner A., Dillmann I., Dollinger G., Lierse von Gostomski Ch., Kossert K., Maiti M., Poutivtsev M. and Remmert A. (2010) A new value for the half-life of ^{10}Be by heavy-ion elastic recoil detection and liquid scintillation counting. *Nuclear Instrum. Meth. Phys. Res. B* **268**, 187–191.

Krause M. O. and Oliver J. H. (1979) Natural widths of atomic K and L levels, K alpha X-ray lines and several KLL auger lines. *J. Phys. Chem. Ref. Data* **8**, 329–338.

Lange R. A. and Carmichael I. S. E. (1987) Densities of Na_2O-K_2O-MgO-MgO-FeO-Fe_2O_3-Al_2O_3-TiO_2-SiO_2 liquids: New measurements and derived partial molar properties. *Geochim. Cosmochim. Acta* **51**, 2931–2946.

Le Maitre R. W., Bateman P., Dudek A., Keller J., Lemeyre J., Le Bas M., Sabine P., Schmid R., Sorensen H., Streckeisen A., Wooley A. and Zanettin B. (1989) *A Classification of Igneous Rocks and Glossary of Terms*. UK, Blackwell Publishing, Oxford, p. 193.

Luguet A., Nowell G. M. and Pearson D. G. (2008) ^{184}Os/^{188}Os and ^{186}Os/^{188}Os measurements by negative thermal ionisation mass spectrometry (N-TIMS): Effects of interfering element and mass fractionation corrections on data accuracy and precision. *Chem. Geol.* **248**, 342–362.

Luguet A., Behrens M., Pearson D. G., König S. and Herwartz D. (2015) Significance of the whole rock Re–Os ages in cryptically and modally metasomatised cratonic peridotites: Constraints from HSE–Se–Te systematics. *Geochim. Cosmochim. Acta* **164**, 441–463.

Ma P., Aggrey K., Tonzola C., Schnabel C., de Nicola P., Herzog G. T., Wasson J. T., Glass B. P., Brown L., Tera F., Middleton R. and Klein J. (2004) Beryllium-10 in Australasian tektites: constraints on the location of the source crater. *Geochim. Cosmochim. Acta* **68**, 3883–3896.

Mader D. and Koeberl C. (2009) Using Instrumental Neutron Activation Analysis for geochemical analyses of terrestrial impact structures: Current analytical procedures at the University of Vienna Geochemistry Activation Analysis Laboratory. *Appl. Radiat. Isot.* **67**, 2100–2103.

Meisel T., Walker R. J., Irving A. J. and Lorand J. P. (2001) Osmium isotopic compositions of mantle xenoliths: A global perspective. *Geochim. Cosmochim. Acta* **65**, 1311–1323.

Morris J. D. and Tera F. (1989) ^{10}Be and ^{9}Be in mineral separates and whole rocks from volcanic arcs: Implications for sediment subduction. *Geochim. Cosmochim. Acta* **53**, 3197–3206.

Ngo H. H., Wasserburg G. J. and Glass B. P. (1985) Nd and Sr isotopic composition of tektite material from Barbados and their relationship to North America tektites. *Geochim. Cosmochim. Acta* **49**, 1479–1485.

Nishiizumi K., Imamura M., Caffee M. W., Southon J. R., Finkel R. C. and McAninch J. (2007) Absolute calibration of ^{10}Be AMS standards. *Nucl. Instru. Meth. Phys. Res. B* **258**, 403–413.

O'Keefe J. A. (1976) *Tektites and their Origin*. Elsevier, Amsterdam, Netherlands, p. 254.

Ostermann M., Deutsch A. and Masaitis V. (1996) Geochemistry and Nd-Sr isotope signature of tektites (indochinites, urengoite) and impact melt glasses (zhamanshinites, irghizites). *Lunar Planet. Sci.* **27**, 987–988.

Patino L. C., Carr M. J. and Feigenson M. D. (1997) Crossarc geochemical variations in volcanic fields in Honduras, C. A.: Progressive changes in source with distance from the volcanic front. *Contrib. Miner. Petrol.* **129**, 341–351.

Patino L. C., Carr M. J. and Feigenson M. D. (2000) Local and regional variations in Central American arc lavas controlled by variations in subducted sediment input. *Contrib. Miner. Petrol.* **138**, 265–283.

Pearson D. G. and Woodland S. J. (2000) Solvent extraction/ anion exchange separation and determination of PGEs (Os, Ir, Pt, Pd, Ru) and Re-Os isotopes in geological samples by isotope dilution ICP-MS. *Chem. Geol.* **165**, 87–107.

Peucker-Ehrenbrink B. and Jahn B. M. (2001) Rhenium-osmium isotope systematics and platinum group element concentrations: Loess and the upper continental crust. *Geochem. Geophys. Geosyst.* **2**, 1061. doi.10.1029/2001GC000172.

Poag C. W., Koeberl C. and Reimold W.U. (2004) Chesapeake Bay crater: Geology and geophysics of a late eocene submarine impact structure. In *Impact Studies*, **vol. 4**, Springer Verlag, Heidelberg, 522 pp (+ CD-ROM).

Povenmire H. (2016) Extending the Belize tektite strewn field. In *47th Lunar and Planetary Science Conference*, abstract no. 1123.

Povenmire H., and Cornec J.H. (2015) The 2014 report on the Belize tektite strewn field. In *46th Lunar and Planetary Science Conference*, abstract no. 1132.

Povenmire H., Harris R.S. and Cornec J.H. (2011) The new Central American tektite strewn field. In *42nd Lunar and Planetary Science Conference* (Abstract) #1224.

Povenmire H., Burrer B., Cornec J., and Harris R.S. (2012) The Central American tektites and strewn field update. In: *43rd Lunar and Planetary Science Conference*, abstract no. 1260.

Povenmire H., Cornec J., Cornec L., and Burrer B. (2014) The Central American tektite strewn field – Progress Report 2013. In *45th Lunar and Planetary Science Conference*, abstract no. 1145.

Premo W. R. and Izett G. A. (1992) Isotopic signature of black tektites from the K/T boundary on Haiti: Implications for the age and type of source material. *Meteoritics* **27**, 413–423.

Ricketts S., King, Jr., D. T., Meyers, Sr., N. R. and Larsen D. (2021) Upper Paleocene to Lower Eocene clay deposits of the Red Bank group, northern Belize, Central America. *GeoGulf Transactions* **71**, 225–239.

Rochette P., Gattacceca J., Devouard B., Moustard F., Bezaeva N. S., Cournede C. and Scaillet B. (2015) Magnetic properties of tektites and other related impact glasses. *Earth Planet. Sci. Lett.* **432**, 381–390.

Rochette P., Alaç R., Beck P., Brocard G., Cavosie A. J., Debaille V., Devouard B., Jourdan F., Mougel B., Moustard F., Moynier F., Nomade S., Osinski G. R., Reynard B. and

Cornec () Pantasma: Evidence for a Pleistocene circa 14 km diameter impact crater in Nicaragua. *Meteoritics Planet. Sci.* **54**, 880–901.

Rochette P., Beck P., Bizzarro M., Braucher R., Cornec J., Debaille V., Devouard B., Gattacceca J., Jourdan F., Moustard F. and Moynier F. (2021) Impact glasses from Belize represent tektites from the Pleistocene Pantasma impact crater in Nicaragua. *Commun. Earth Environ.* **2**, 1–8. doi.10.1038/s43247-021-00155-1.

Rossano S., Balan E., Morin G., Bauer J. P., Calas G. and Brouder C. (1999) ^{57}Fe Mössbauer spectroscopy of tektites. *Phys. Chem. Minerals* **26**, 530–538.

Rudnick R. L. and Gao S. (2003) Composition of the continental crust. In *The Crust*, **vol. 3** (ed. R. L. Rudnick). Elsevier. pp. 1–64.

Schulz T., Sackl F., Fragner E., Luguet A., van Acken D., Abate B., Badjukov D. D. and Koeberl C. (2020) The Zhamanshin impact structure, Kazakhstan: A comparative geochemical study of target rocks and impact glasses. *Geochim. Cosmochim. Acta* **268**, 209–229.

Schwarz W. H., Trieloff M., Bollinger K., Gantert N., Fernandes V. A., Meyer H. P., Povenmire H., Jessberger E. K., Guglielmino M. and Koeberl C. (2016) Coeval ages of Australasian, Central American and Western Canadian tektites reveal multiple impacts 790 ka ago. *Geochim. Cosmochim. Acta* **178**, 307–319.

Senftle F. E., Thorpe A. N., Grant J. R., Hildebrand A., Moholy Nagy H., Evans B. J. and May L. (2000) Magnetic measurements of glass from Tikal, Guatemala: Possible tektites. *J. Geophys. Res.: Solid Earth* **105**, 18921–18925.

Serefiddin F., Herzog G. F. and Koeberl C. (2007) Beryllium-10 concentrations of tektites from the Ivory Coast and from Central Europe: Evidence for near-surface residence of precursor materials. *Geochim. Cosmochim. Acta* **71**, 1574–1582.

Shaw H. and Wasserburg G. J. (1982) Age and provenance of the target materials for tektites and possible impactites as inferred from Sm-Nd and Rb-Sr systematics. *Earth Planet. Sci. Lett.* **60**, 155–177.

Stecher O., Ngo H. H., Papanastassiou D. A. and Wasserburg G. J. (1989) Nd and Sr isotopic evidence for the origin of tektite material from DSDP Site 612 off the New Jersey Coast. *Meteoritics* **24**, 89–98.

Tagle R. and Berlin J. (2008) A database of chondrite analyses including platinum group elements, Ni Co, Au, and Cr: Implications for the identification of chondritic projectiles. *Meteoritics Planet. Sci.* **43**, 541–559.

Völkening J., Walczyk T. and Heumann K. G. (1991) Osmium isotope ratio determinations by negative thermal ionization mass spectrometry. *Internat. J. Mass Spectrom. Ion Proc.* **105**, 147–159.

Vogt S. and Herpers U. (1988) Radiochemical separation techniques for the determination of long-lived radionuclides in meteorites by means of accelerator mass spectrometry. *Fresenius Z. Anal. Chemie* **331**, 186–188.

Walker J. A., Patino L. C., Cameron B. I. and Carr M. J. (2000) Petrogenetic insights provided by compositional transects across the Central American arc: Southeastern Guatemala and Honduras. *J. Geophys. Res.* **105**, 18949–18963.

Walker J. A., Patino L. C., Carr M. J. and Feigenson M. (2001) Slab control over HFSE depletions in Central Nicaragua. *Earth Planet. Sci. Lett.* **192**, 533–543.

Wilke M., Farges F., Petit P. E., Brown G. E. and Martin F. (2001) Oxidation state and coordination of Fe in minerals: an Fe K-XANES spectroscopic study. *Am. Mineral.* **86**, 714–773.

Willenbring J. K. and von Blanckenburg F. (2010) Long-term stability of global erosion rates and weathering during late-Cenozoic cooling. *Nature* **465**, 211–214.

Associate editor: Yuri Amelin